THESIS FOR THE DEGREE OF LICENTIATE OF ENGINEERING

Millimeter-Wave High-Gain Antenna for 5G Backhauling with Auto-beam-tracking Function

Enlin Wang

CHALMERS
UNIVERSITY OF TECHNOLOGY

Department of Electrical Engineering
Chalmers University of Technology
Gothenburg, Sweden, 2023

Millimeter-Wave High-Gain Antenna for 5G Backhauling with Auto-beam-tracking Function

Enlin Wang

Department of Electrical Engineering
Chalmers University of Technology
SE-412 96 Gothenburg, Sweden
Phone: +46 (0)31 772 1000
www.chalmers.se

Printed by Chalmers Reproservice
Gothenburg, Sweden, December 2023

To my family

Abstract

As microwave links are increasingly deployed within the millimeter-wave frequency range, E-band (70/80 GHz) links have been installed on a global scale. One major technological challenge in this high-frequency spectrum is the significant increase in path loss between receivers and transmitters. To address this issue, antennas with a larger aperture and higher gain are commonly employed. Unfortunately, these antennas feature an extremely narrow beamwidth, making alignment exceedingly difficult and potentially compromising link reliability, especially when the supporting mast of the antenna experiences swaying, disturbances, or twisting. This issue has emerged as a significant challenge in current high-frequency communication system, urgently requiring a perfect solution. This thesis introduces several ultra-high gain dual-reflector antennas that utilize feed defocusing technology for beam steering to address link disruption caused by mast sway, specifically designed for 5G backhaul applications.

Firstly, two types of monopulse antennas are presented: 1. A dual-polarized monopulse antenna based on a planar magic-T structure, which reduces manufacturing complexity due to the use of gap waveguide (GW) structures. The feed system provides SUM and DIFF beams for data transmission and tracking, respectively. 2. A dual-polarized monopulse antenna based on phase shifters and couplers, where phase compensation technology is employed to achieve DIFF beam steering. As part of the design, three compact, low-loss, reconfigurable phase shifters based on GW technology have been developed. These phase shifters achieve varying rates of phase change through the adjustment of the lengths of the transmission lines and the dimensions of slow-wave structures. To achieve precise beam tracking, an electromechanical automatic control system has been designed for these antennas. All measured outcomes have closely validated our theoretical forecasts.

Secondly, in order to have a low-cost solution without using DIFF receivers for tracking, a dual-reflector antenna system with beam steering through feed defocusing has been developed. Our design goal is to avoid the use of coaxial cables for connections between the defocusing movable feed and the Tx/Rx ports since the cable connection leads to cable bending, reduced reliability, and increased likelihood of failure. For this purpose, we propose 1D and 2D mechanically movable feeds combined with a Gregorian reflector. In this design, we first introduce three types of reconfigurable transmission lines: shielded

rectangular waveguides, movable rectangular waveguides, and universal-joint circular waveguides. These innovations extend the applications of GW technology into the mechanically reconfigurable domain. For precise beam tracking capabilities, two cost-effective and environmentally sustainable mechanical tracking mechanisms are proposed: a gravity-driven balance system and a gravity-driven spring system. All measurement results closely confirm our theoretical predictions.

Finally, this thesis proposes other two innovative GW structures: 1. A novel concept of patterned distributed pins designed to stabilize the phase performance of Half-Mode Gap Waveguides, even with manufacturing inaccuracies, thus streamlining manufacturing processes. 2. A newly developed Ball-pen GW, which utilizes commercially available low-cost pens for mechanical reconfigurability, offering an easily manufacturable solution.

In summary, the techniques and solutions presented in this thesis aim to offer a strategic approach to addressing the challenges encountered in 5G backhaul systems and other mmWave antenna systems. It is our aspiration that these advancements will contribute to the optimization and enhancement of backhaul networks.

Keywords: Ultra-high-gain antenna, 5G backhaul, auto-beam-tracking, mechanical movement, gap waveguide.

List of Publications

This thesis is based on the following publications:

[A] **E. Wang**, J. Yang, A. U. Zaman, "An E-band reconfigurable phase shifter based on gap waveguide". *2022 16th European Conference on Antennas and Propagation (EuCAP)*, Madrid, Spain, Mar. 2022 .

[B] **E. Wang**, T. Zhang, A. U. Zaman, T. Emanuelsson, P. Thorsen, S. Agneessens, J. Yang, "A compact gap-waveguide dual-polarized Ka-band feed for 50 dBi reflector antennas with tracking function". *IEEE Access*, vol. 10, pp. 91622-91630, Aug. 2022 .

[C] **E. Wang**, S. Agneessens, A. U. Zaman, H. Karlsson, Z. Yan, J. Yang, "E-band low-loss reconfigurable phase shifters". *IEEE Microwave and Wireless Technology Letters*, vol. 33, no. 7, pp. 999-1002, Mar. 2023 .

[D] **E. Wang**, A. U. Zaman, Z. Yan, J. Yang, "Pattern distributed pins in half-mode groove gap waveguide for stable performance and low cost". *2023 17th European Conference on Antennas and Propagation (EuCAP)*, Florence, Italy, 2023 .

[E] **E. Wang**, S. Agneessens, O. Talcoth, C. Bencivenni, A. U. Zaman, J. Yang, "Applications of contactless characteristics of gap waveguides in mechanical reconfigurability". *2023 International Symposium on Antennas and Propagation (ISAP)*, Kuala Lumpur, Malaysia, Oct. 2023 .

[F] **E. Wang**, A. U. Zaman, Z. Yan, J. Yang, "Low-cost ball-pen gap waveguide with nearly zero friction for reconfigurable movements". *IEEE Microwave and Wireless Technology Letters*, vol. 33, no. 11, pp. 1580-1583, Sep. 2023 .

[G] **E. Wang**, S. Agneessens, O. Talcoth, L. Manholm, C. Bencivenmi, E. Alfonso, A. Wennergren, H. Stalrud, A. U. Zaman, and J. Yang, "A 50 dBi E-band dual-reflector antenna for 5G backhauling with auto-beam-tracking function". *Submitted to IEEE Transactions on Antenna and Propagation* .

[H] **E. Wang**, A. Wennergren, H. Stalrud, C. Bencivenmi, E. Alfonso, A. U. Zaman, and J. Yang, "Antenna and mechanical co-design for auto-beam-tracking

in backhaul systems". *Submitted to 18th European Conference on Antennas and Propagation* .

Other publications by the author, not included in this thesis, are:

[I] **E. Wang**, T. Zhang, A. U. Zaman, T. Emanuelsson, P. Thorsen, S. Agneessens, J. Yang, "Monopulse feeding network based on new gap waveguide planar magic-tees". *2022 International Symposium on Antennas and Propagation (ISAP)*, Sydney, Australia, Oct. 2022.

[J] **E. Wang**, S. Agneessens, M. Hasselblad, A. U. Zaman, J. Yang, "A 50 dBi dual-reflector E-band antenna for 5G backhaulings with beam steering function". *2023 Swedish Microwave Days (SMWD)*, Stockholm, Sweden, May. 2023.

Acknowledgments

First and foremost, I express my deepest and enduring gratitude to my supervisor, Prof. Jian Yang. He has offered me not only the rare opportunity to embark on my Ph.D. journey but has also guided me through every significant milestone with wisdom and deliberate action. Throughout this rich and intricate academic odyssey, he has played multiple roles—mentor, guide, and even a beacon of light in my life. His expert guidance, mentorship, and unwavering support have been instrumental in shaping both my research work and academic growth. Every meeting and discussion with him has been a collision of wisdom, where he patiently but firmly guides me through my errors and blind spots, always urging me to find a better solution. He is not only an essential mentor on my academic growth journey but also a priceless treasure in my life journey.

I also wish to express my gratitude to my examiner, Prof. Marianna Ivashina. Whenever I encountered challenges or hit bottlenecks in my research, her radiant smile and empowering words never failed to reignite my self-confidence and determination. Additionally, I owe a special debt of thanks to Associate Prof. Ashraf Uz Zaman. His invaluable academic suggestions have consistently served as a catalyst for new ideas and directions in my research endeavors. My profound gratitude also goes to Prof. Rob Maaskant, along with Senior Researchers Dr. Pavlo Krasov, Dr. Oleg Iupikov, and Dr. Artem Vilenskiy. Their professional support and insightful contributions have greatly expanded my academic horizon, for which I am profoundly respectful and grateful. Special thanks go to Pavlo for his invaluable assistance during the antenna measurements.

As an industrial Ph.D. student jointly trained by Chalmers and Gapwaves AB, I cannot express enough how grateful I am for the unwavering support extended by Gapwaves AB. Special thanks are in order for my co-supervisor, Dr. Carlo Bencivenni and Dr. Abbas Vosoogh. They have not only imparted comprehensive and insightful academic guidance but have also masterfully intertwined theoretical research with real-world industrial demands. This unique approach has allowed me to experience the rigors of scientific investigation while deepening my understanding of the myriad challenges and opportunities that exist in the industrial sector.

For all the partners involved in the 50 dBi project, I am profoundly grateful. Their professional dedication and selfless support provided me with a unique

platform for learning and growth. I deeply appreciate their collaborative spirit and shared vision. Special thanks to Dr. Sam Agneessens, Dr. Oskar Talcoth, Lars Manholm, Thomas Emanuelsson, and Per-Arne Thorsén from Ericsson, as well as Marcus Hasselblad, Anders Wennergren, Dr. Esperanza Alfonso, Daniel Johansson, Hanna Karlsson, and Henrik Stalrud from Gapwaves AB. Their unrestrained assistance immensely contributed to my development in this project.

Throughout my academic journey, the unwavering support from my colleagues has been invaluable. I'd like to extend my heartfelt thanks to the entire Electrical Engineering Department for fostering an environment brimming with camaraderie and inspiration. Special thanks to my office mates Prabhat, Jin, Theodoros, and Mu who have always been there to assist whenever I faced challenges; their presence made my office life all the more pleasant. Additionally, I thank my friends from the Antenna Group: Qiannan, Zhaorui, Juan Luis, Yingqi, Raha, Teanette, Yuqing, Usman, Viktor, Mustafa, Nazanin, Dijun, and Iaroslav for their support during and after work hours. I'm also deeply grateful to visiting researchers, Prof. Ahmed Kishk, Fan, Bin, Songtao, Liangyu, David, Longhui, Wenjing, and Shigang, who have been immensely helpful.

Last but most certainly not least, I extend my deepest gratitude to my parents and husband, who have consistently stood behind me with unwavering support and boundless love, regardless of the choices and challenges I've faced. Thank you for being my rock and my sanctuary, where I find the courage to strive for excellence.

In closing, I wholeheartedly thank everyone who has contributed to my journey in any capacity. Each act of kindness and every morsel of support have coalesced into a formidable force that propels me forward, imbuing my path into the future with renewed determination and unwavering resolve.

Enlin
Göteborg, Dec. 2023

Acronyms

2D/3D:	Two/Three dimensional
5G:	Fifth generation
ABS:	Absorber
AMC:	Artificial magnetic conductors
BFNs:	Beamforming networks
CNC:	Computer numerical control
CP:	Circularly polarized
DBF:	Digital beam forming
DF:	Direction finding
DPDT:	Dual-pole dual-throw
E-GGW:	E-plane groove gap
EBG:	Electromagnetic band-gap
EM:	Electromagnetic
ETSI:	European telecommunications standards institute
GGW:	Groove gap waveguide
GW:	Gap waveguide
HM-GGW:	Half-mode groove gap waveguide
HPBW:	Half power beamwidth
IMBW:	Impedance bandwidth
IMGW:	Inverted microstrip gap waveguide
IoT:	Internet of things

LP:	Linearly polarized
LTCC:	Low-temperature co-fired ceramic
mmWave:	Millimeter wave
M-reconfiguration:	Mechanical reconfiguration
MEMS:	Microelectromechanical systems
MIMO:	Multi input multi output
OMT:	Orthogonal mode transducer
PCB:	Print circuit board
PEC:	Perfect electric conductor
PMC:	Perfect magnetic conductor
RGW:	Ridge gap waveguide
RLSAs:	Radial line slot arrays
RX:	Receivers
SIW:	Substrate integrated waveguide
TL:	Transmission line
TX:	Transmitters
UHG:	Ultra-high gain

Contents

Part I

Overview

CHAPTER 1

Introduction

1.1 Motivation

In the era of widespread digitalization and internet accessibility, wireless communication technology serves as an essential catalyst in bridging interpersonal connections as well as facilitating the Internet of Things (IoT) and mobile communication systems [1], [2]. Accompanying the rapid advancements in these domains is the escalating demand for high-speed, low-latency, and reliable communication links. Fifth Generation (5G) technologies and their subsequent iterations offer compelling solutions to these challenges, boasting remarkable performance enhancements such as data transmission rates of up to 10 Gb/s (compared to 1 Gb/s on 4G) and ultra-low latency as minimal as 1 ms (compared to about 70 ms on today's 4G networks)[3], [4]. However, the realization of these sophisticated capabilities is far from trivial. It requires not only intricate designs of communication protocols but also robust support at the physical layer. Among these, hardware design, particularly the antenna system, stands out as crucial. It serves as an indispensable component in ensuring the high performance and reliability of networks.

Millimeter-wave (mmWave) bands, especially the E-band (71-76 GHz/81-86

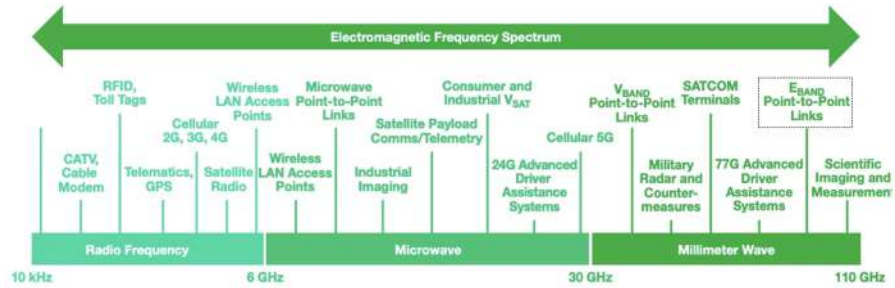

Figure 1.1: Millimeter wave spectrum overview. [5]

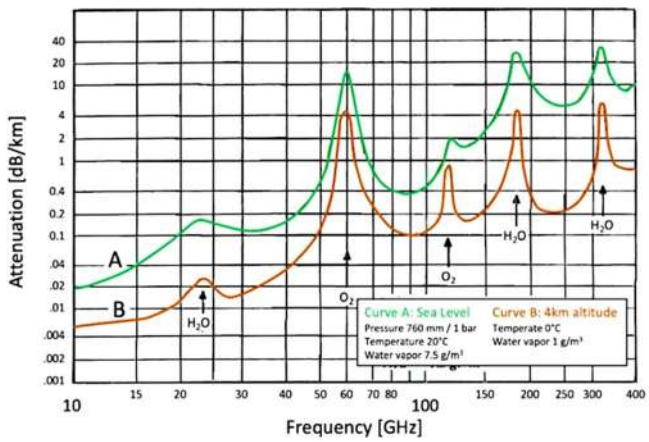

Figure 1.2: Atmospheric attenuation (units = dB/km) for air as a function of radio frequency (shown from 10 to 400 GHz) for two different conditions - one at sea level (green) and another at an altitude of 4km (brown). [6]

GHz), is highly regarded for its high-speed performance, flexibility, and abundant spectrum resources, with the capacity to increase mobile infrastructure capabilities by fivefold, thereby meeting the transmission requirements of 5G. This advantage has facilitated the widespread adoption of the E-band, establishing it as one of the three principal spectrums deployed globally in 2020 [8], [9]. Within the context of 5G mmWave applications, the E-band demonstrates substantial potential in point-to-point backhaul communication, as illustrated in Fig. 1.1. Despite these advantages, E-band and mmWave communications

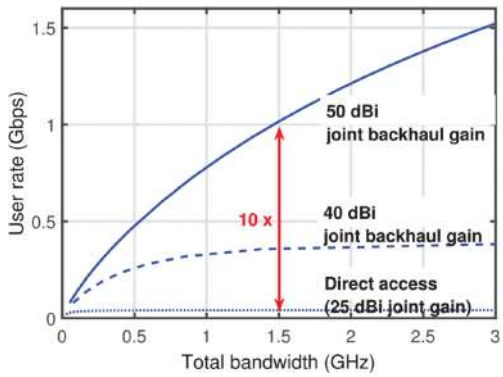

Figure 1.3: Per user throughput (in total 5 users) as a function of total bandwidth (Backhaul + Access) for the single-hop "star-network" backhaul topology. With high directional gain of 50 dBi for backhaul links provides 1 Gbps per user throughput, which is more than 10 times faster than direct access (i.e., no relaying) where the joint transmit-receive antenna gain is assumed to be 25 dBi. If the combined array gain for backhaul links falls short to 40dBi due to scattering, the rate gain falls to less than 400 Mbps/user. [7]

face a host of challenges[10]. These include: 1) Path loss and fading: mmWave signals are subjected to higher levels of path loss and multipath fading during transmission, contributing to drastic variations in signal strength and thereby compromising the stability and reliability of the communication link. According to the Friis transmission equation, the higher the frequency, the more the radio signals attenuate during propagation. For instance, a communication link at 80 GHz experiences 20 dB more attenuation compared to an 8 GHz link of the same length. 2) Atmospheric absorption and rain attenuation: The absorbent properties of mmWave signals in atmospheric conditions, exacerbated under rainy conditions, impose further limitations on communication distance and reliability, as shown in Fig. 1.2. One way to address this challenge is to deploy more transmission towers to expand the number of point-to-point systems, but this is not economically viable. Another solution is the use of ultra-high gain antennas ($\geq$ 50 dBi) operating in mmWave spectrum (as shown in Fig. 1.3), which are key to achieving sustainable long-distance 5G mmWave backhaul systems [7].

In summary, within this context, ultra-high-gain antenna technology emerges

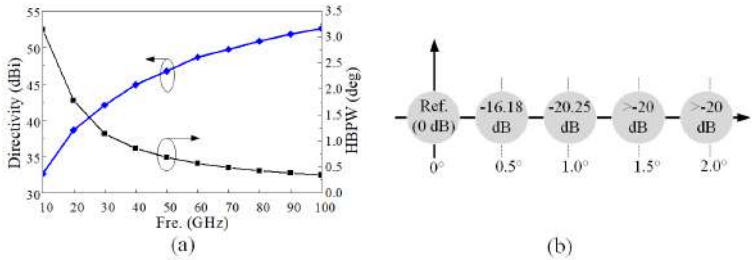

Figure 1.4: 0.6 m Gregorian dual-reflector antenna. (a) Theoretical directivity and HPBW. (b) Power loss caused by antenna misalignment.

as an indispensable element in mitigating the challenges of 5G millimeter-wave communications. These antennas are capable of compensating for path losses during signal propagation and providing substantial signal enhancement, thereby ensuring reliable data transmission.

1.2 Research Challenges

Ultra-High Gain Antennas ($\geq$ 50 dBi) encounter a variety of design and implementation challenges. These specific challenges include: 1. Ultra-high gain necessitates that antennas maintain high radiation efficiency and low ohmic losses at large-aperture mmWave frequencies. 2. The antenna bandwidth needs to cover the entire E-band spectrum. 3. Achieving compact dual-polarization [11], [12]. 4. To address the issue of gain reduction due to beam misalignment in narrow beams, the sensitivity of beam width is critical, as illustrated in Fig. 1.4. In this figure, a 0.6-meter Gregorian reflector achieves an approximate gain of 50 dBi at 70 GHz. Under these circumstances, the half-power beam width (HPBW) is around 0.5°. A deviation from the beam's center by $\pm 2°$ results in a reduction of gain by more than 20 dB, highlighting the antenna's high sensitivity to disturbances such as wind-induced vibrations and mast swings. 5. Given the high throughput and low latency requirements of 5G networks, point-to-point backhaul infrastructure must facilitate rapid and accurate data transmission. 6. Both the antenna and its tracking servo system require high performance while also being cost-effective.

Regarding the fourth challenge, multiple reports have noted the sensitivity

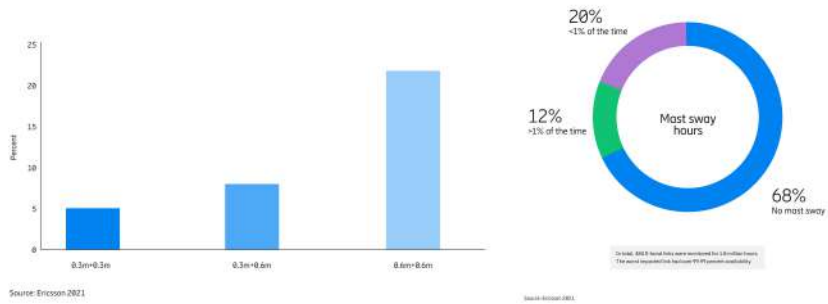

(a) (b)

Figure 1.5: (a) Antenna configurations for links impacted by mast sway more than 1 percent of the time. (b) E-band links monitored for 1.8 million hours).[13]

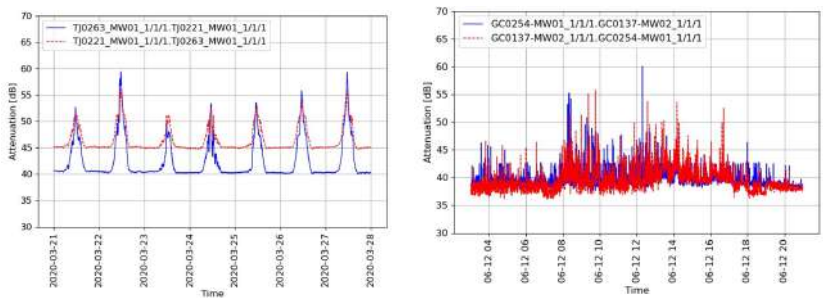

(a) (b)

Figure 1.6: Measured E-band link attenuation due to wind-induced sway, thermal deformations, and sunflower effect in common mast structure. (a) Thermal deformations. (b) Wind-induced sway in an unstable structure. [13]

of the mast to external factors such as wind, rain, and snow [13]. A comprehensive year-long study carried out by Ericsson monitored 484 links for mast swing within the network. The study considered various antenna sizes: 46% employed 0.3 m antennas on both ends, 37% used 0.6 m antennas, and the remaining 17% used a combination of both. Results, depicted in Fig. 1.5(a),

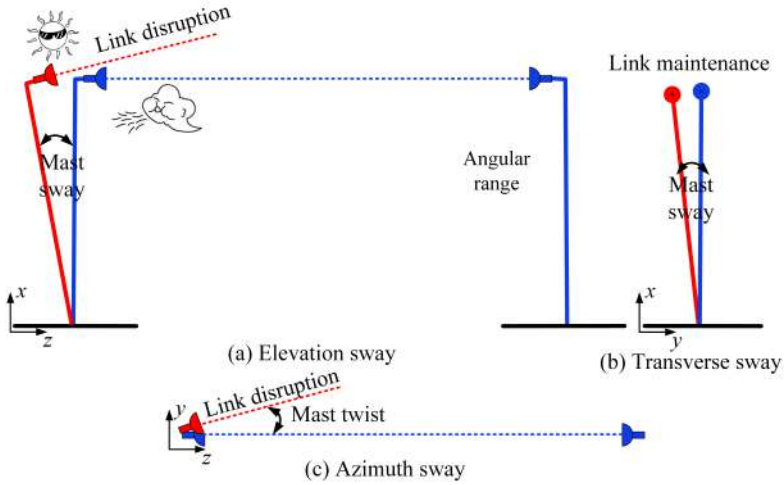

Figure 1.7: Illustration of mast oscillation.

show that links with 0.6 m larger antennas (22% swing likelihood) are more susceptible to mast swing compared to those with 0.3 m smaller antennas (5% swing likelihood). Additionally, during the 1.8 million hours of cumulative monitoring, approximately 0.4% (or 7828 hours) exhibited varying degrees of mast swing. Specifically, about two-thirds (68%) showed no significant mast swing, while one-third detected some swing, with 12% exceeding a 1% swing, as illustrated in Fig. 1.5(b).

Further investigation revealed two scenarios for mast swing:

- Slow swing at a rate of 2-deg per day, which is induced by thermal expansion due to sunlight exposure, causing deformations in the antenna mounting structure, as shown in Fig. 1.6(a).
- Rapid swing at rates of 2-deg per 0.5-1 second, potentially due to vibrations from passing large trucks or strong wind loads, as depicted in Fig. 1.6(b).

A mast sway can be decomposed into three orthogonal movements as shown in Fig. 1.7: 1) the elevation sway occurs when the antenna rotates around the y-axis, causing the beam to point up or down away from the z-axis (the link

direction); 2) the transverse sway happens when the antenna rotates around the z-axis, resulting in only a small position offset for the beam without changing its overall pointing direction; 3) the azimuth sway, often referred to as the twist, occurs when the antenna rotates around the x-axis, causing the beam to point to the right or the left in azimuth away from z-axis. The transverse sway does not alter the beam's pointing direction. The twist (mainly due to thermal deformation) happens with much less amplitude and occasions than the elevation sway [14].

In summary, both rapid wind-induced swings and slow thermal deformations could lead to a path loss increase of more than 20 dB, severely impacting data transmission rates and potentially causing link failure. Therefore, E-band broadband dual-polarization ultra-high gain antennas with real-time tracking capabilities are considered key for successful deployment in large-capacity 5G backhaul systems.

1.3 High-Gain Antenna Types

Based on our current understanding and market analysis, there is a noticeable absence of commercially available antenna products with 50 dBi gain that also offer beam tracking capabilities, particularly in the frequency range of 70 GHz and above. Additionally, published research that investigates antennas with 50 dBi gains at 70 GHz or higher is remarkably sparse.

A few ultra-high-gain antennas have been reported: Fig. 1.8(a) portrays a large offset reflector with a large array feed (100 elements) with 50 dBi gain was proposed in [15] at 30 GHz. However, the large-sized reflector and the offset geometry make the mounting and possible realization of the beam steering function very expensive. Lens antenna is an alternative for achieving 50dBi+, 70GHz+ antennas, such as the lens antennas in [16], [20], [21], as illustrated in Fig. 1.8(b). Problems for lens antennas are the high cost of manufacturing and heavy weight for 50 dBi gain antennas that require a large volume. Recently, a new type of high-gain antenna at 30 GHz, called meta-surface antenna [17], has been reported, depicted in Fig. 1.8(c). The 30 GHz meta-surface antenna has achieved 38 dBi gain and potentially 50 dBi gain with low profile realized by low-cost printed circuit board manufacturing technique. Disadvantages of the meta-surface antennas includes: only single circular polarization realization, very narrow bandwidth and no beam steering function (though multibeam can

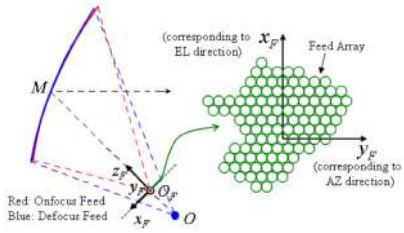

(a) Offset reflector with feed array [15]

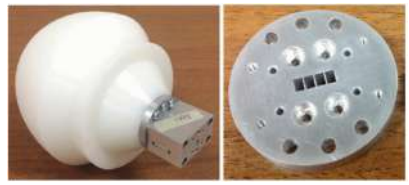

(b) Lens antenna [16]

(c) Metasurface antenna [17]

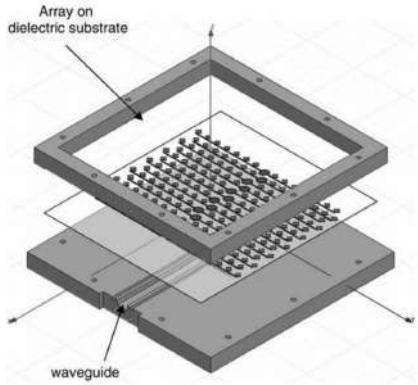

(d) Printed antenna [18]

(e) Reflectarray antenna [19]

Figure 1.8: Different forms of high-gain antennas

be realized). In addition, as shown in Fig. 1.8(d), the printed array antenna has inherently low radiation efficiency due to high ohmic loss in microstrip lines and substrates at mmWs. The example in [18] has achieved 30 dBi at 30 GHz with 69% radiation efficiency, which indicates that the radiation efficiency will be below 50% at 70 GHz and, therefore, it is very difficult to achieve 50 dBi gain in the mmW regime. Another alternative is the reflect-arrays, such as the one presented in Fig. 1.8(e) and cited in [19], where 42.3 dBi gain was achieved with a 30 cm diameter antenna at 75 GHz. Unfortunately, this type of solution suffers from limited bandwidth and high cost to have beam auto-tracking function.

After extensive comparison and research, in this thesis, we choose to use reflector antennas as the solution to the challenges faced in backhaul antenna systems. The ohmic losses in reflector antennas are minimized, and by using a dual-reflector configuration, a gain exceeding 50 dBi can be achieved through a more compact reflector design.

To implement the automatic beam steeing function in a simple way, modifications can be made to the antenna system configuration. For example, beam tracking can be achieved by moving the reflector. However, cumbersome mechanical systems yield sluggish response times that are unsuitable for rapid steering needs. In the case of dual-reflector antennas, one alternative is to move the sub-reflector, which necessitates the displacement of much smaller mass. However, one drawback of a dual-reflector system is that the sub-reflector and its supporting structure effectively reduce the aperture of the antenna, since it is situated in front of the main reflector [22]. This issue is exacerbated when adding the requisite mechanical components (motors, cables, additional supports) to mobilize the sub-reflector. The problem becomes even worse if all these additional elements are placed behind the sub-reflector, thereby making the antenna excessively heavy. Given the increasing demands of modern tracking technologies for high performance, low cost, and fast scanning, beam steering through feed movement offers the simplest solution. With the feed distributed behind the main reflector, beam steering can be easily achieved by merely repositioning the feed [23]. This approach greatly relaxes the constraints on the mechanical tracking servo system, which can be installed behind the feed without adversely affecting the antenna's radiation performance.

The three types of equilibrium states of the Gregorian reflector antenna with

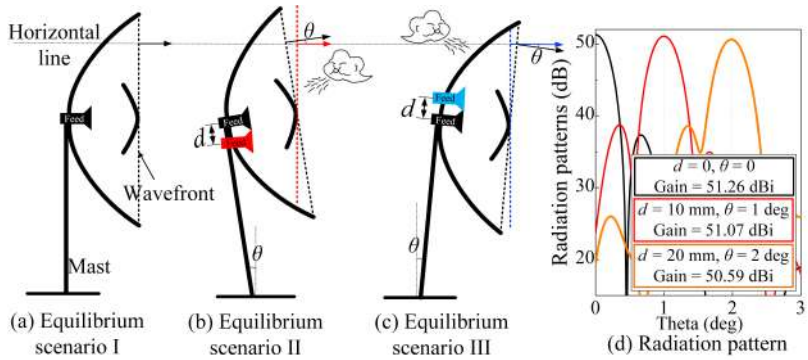

Figure 1.9: Schematic of beam compensation during mast oscillation.

beam control are shown in Fig. 1.9, where Fig. 1.9(a) displays the antenna's beam orientation under stable conditions. When the mast tilts to the left, as shown in Fig. 1.9(b), the beam shifts upward (indicated by a black arrow). At this point, by moving the feed downward (marked in red), the beam can be recalibrated to the horizontal direction. Similarly, as demonstrated in Fig. 1.9(c), when the mast leans to the right, the beam deflects downward (shown by the black arrow). By elevating the feed (denoted in blue), the beam can be realigned horizontally. The relationship between the feed movement distance and the beam deviation is dictated by the reflector's configuration. In this study, the chosen setup adheres to the equation $d = 10 \times \theta$, where d represents the displacement of the feed in mm, and θ denotes the beam deviation angle in degree.

1.4 Gap Waveguide Technology

Gap waveguide (GW) technology, initially proposed in 2008 [28], has garnered widespread research interest over the past decade due to its advantages such as low loss and simplified manufacturing processes. It shows particular promise for applications in high-frequency, high-power, and mmWave systems [29]–[33]. The operating principle of GW technology involves the use of Perfect Electric Conductors (PEC) and Artificial Magnetic Conductors (AMC) to confine electromagnetic fields between conductive plates in a narrow gap.

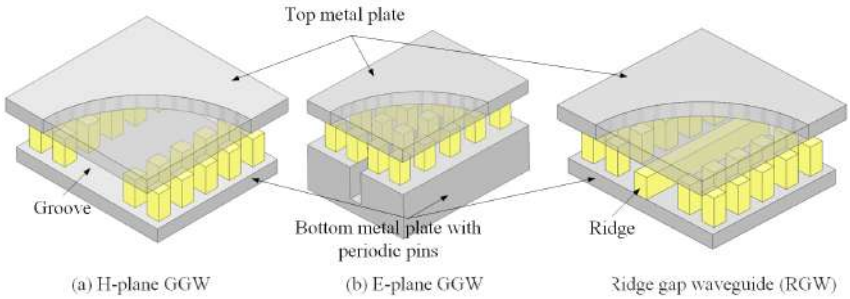

Figure 1.10: Different types of gap waveguide.

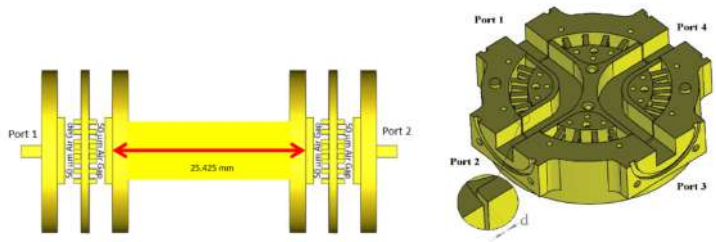

(a) Double-sided pin-flange gap adapters. (b) Waveguide switch [25] [24]

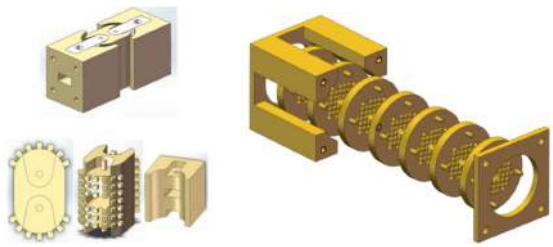

(c) Flexial waveguide transmition line [26] (d) Printed antenna [27]

Figure 1.11: Different forms of contactless structure.

Unlike traditional waveguides, which require strict tolerances and complex joints to prevent leakage, GW naturally suppress radiation and surface wave losses, resulting in higher performance and simpler designs. Various types of

GW exist, as shown in Fig. 1.10, including Ridge Gap Waveguide (RGW), Groove Gap Waveguide (GGW) and so on.

Aside from the aforementioned benefits, a distinctive feature of GW technology is its utilization of "gap". In conventional rectangular waveguides, such gaps typically result in energy leakage and are thus avoided. However, in GW designs, these gaps are not only permissible but can be intentionally "exploited" [24]–[27], [34].

In [24], researchers have leveraged this "gap" feature to design an adapter, as illustrated in Fig. 1.11(a), effectively overcoming a range of challenges associated with high-frequency structure measurements. Normally, good electrical contact requires flanges to be tightly and evenly fastened to the device under test, a potentially time-consuming process, especially for repeated measurements. Yet, with GW technology, even the presence of gaps at the connection points does not result in energy leakage. In [25], a novel dual-pole dual-throw (DPDT) waveguide switch designed for high-power and low-loss applications is introduced, as depicted in Fig. 1.11(b). In [26], a cylindrical non-contact flange is proposed, as shown in Fig. 1.11(c). Similarly, in [27], a real-time rotatable rectangular waveguide design is described. Here, electromagnetic waves are effectively confined within the rectangular waveguide as long as the air gap between two flanges does not exceed the maximum allowable distance, as shown in Fig. 1.11(d). In summary, the "utilization" of these "gaps" remains an intriguing avenue for exploration.

1.5 Scientific Contributions of Thesis

The aim of this thesis is to address the challenges in the field of mmWave point-to-point backhaul communication system by proposing a series of innovative solutions to demonstrate the feasibility of a novel dual-reflector GW feed solution to meet the technical challenges of antennas with gains exceeding 50 dBi above 70 GHz, thereby enhancing the performance and reliability of mmWave communication systems. The innovations of this thesis include:

- A dual-polarized Ka-band feed based on GW technology has been proposed for ultra-high gain reflector antennas. The research employs two planar magic-T structures, achieving a compact dual-layer feeding network for the SUM and DIFF beams used in data transmission and tracking. (presented in **Paper B**)

- The proposal of a tracking technology based on phase compensation and the design of a broadband compact monopulse feed based on phase shifters and couplers. Three reconfigurable phase shifters have been designed to achieve phase compensation. (presented in **Paper A,C**)

- The introduction of a new concept of pin distribution pattern structure to improve the phase performance stability when the Half-Mode Gap Waveguide (HM-GGW) experiences misalignments, thereby reducing manufacturing costs. (presented in **Paper D**)

- The proposal of three types of reconfigurable transmission lines (sheath rectangular waveguide, movable rectangular waveguide, and universal-joint circular waveguide) to extend the applications of GW technology in the field of mechanical reconfigurability. (presented in **Paper E**)

- The introduction of an ultra-high gain E-band dual-reflector antenna system for 5G backhaul, with 1D and 2D beam tracking achieved through defocusing. The feed defocusing is realized by offsetting the feed from its focal point while maintaining a fixed interface with the node (or radio) using a movable gap waveguide configuration. (presented in **Paper F**)

- The proposal of a novel easy-to-manufacture ball-pen GW that utilizes commercially available low-cost ball pens to achieve mechanical reconfigurability. (presented in **Paper G**)

- Integrating the design of the antenna and mechanical structure, three automatic beam tracking methods have been proposed: a sensor-motor-based control method, a gear-driven compensation method by using a secondary mast as a reference, and a gravity-driven pendulum method that leverages gravitational force as the reference, addressing the electromechanical co-design challenges of beam alignment in ultra-high-gain antennas caused by mast sway. (presented in **Paper H**)

According to our estimates, these innovations could reduce the backhaul tower footprint by 50%-60% through our new electromechanical tracking E-band 50 dBi antenna technology, using our UHG antenna, thereby improving the current backhaul tower layouts.

1.6 Thesis Outline

In **Chapter 1**, a overview of the entire research focus is provided, accompanied by an introduction to the primary objectives of the study.

In **Chapter 2**, the background of monopulse antennas is initially presented. This is followed by an introduction to monopulse antenna designs based on Magic-T technology, encompassing two types of planar Magic-T configurations as well as monopulse comparators. Subsequently, the chapter peresent monopulse antenna designs utilizing phase shifters. Additionally, concepts related to sensor-motor tracking systems and pin distribution patterns are discussed.

In **Chapter 3**, the chapter begins by outlining the requirements for antenna design and proceeds to introduce a design featuring automatic 1D beam tracking capabilities. This involves the design of non-contact microwave components and a gravity-driven system for beam steering. Following this, the chapter shows antenna designs with automatic 2D beam tracking functionalities, as well as a gravity-driven spring system for beam steering in auto-tracking setups.

Chapter 4 provides a brief summary of each paper included.

Finally, **Chapter 5** elucidates the directions for future research.

CHAPTER 2

High-Gain Dual-Polarization Monopulse Antennas

2.1 Research Background of Monopulse Antennas

As elaborated in **Section** 1.3, reflector antennas have demonstrated their indispensable advantages in the domain of backhaul systems. To address the specialized requirements associated with mmWave tracking antenna applications, Direction Finding (DF) techniques have emerged as a primary consideration, particularly for determining the line-of-sight direction in point-to-point wireless links. In contrast to conventional tracking methodologies, monopulse tracking has achieved widespread acceptance due to its high level of precision [35]. In addition, in complex electromagnetic environments, radar systems not only necessitate robust anti-interference capabilities but also require the ability to extract target information in the polarization domain. Consequently, dual-polarized monopulse antennas have assumed increased significance compared to their single-polarized counterparts. Such antennas are capable of generating SUM and DIFF patterns with two orthogonal polarizations on both the azimuth and elevation planes, and arbitrary polarizations can be achieved through vector synthesis techniques.

Generally speaking, a monopulse antenna system is composed of two main

components: a comparator serving as SUM and DIFF feed networks, and radiating elements. These comparators are typically constituted of 3 dB couplers, phase shifters, or Magic-T structures [36]–[46]. Comparators utilizing Magic-T architectures facilitate frequency-insensitive in-phase or anti-phase outputs, thereby finding extensive applications in beamforming networks (BFNs), monopulse systems, and discriminators. However, the Magic-T structure, as a 3D component, adds complexity to the antenna system. Moreover, although feeding networks can also be comprised of phase shifters and couplers, many phase shifters demonstrate poor phase balance within specific frequency ranges, thereby compromising performance. To address these challenges, this chapter proposes two innovative designs of high-gain, dual-polarized, wideband monopulse antennas, and offers a complete solution for beam tracking.

2.2 Monopulse Antenna Based on Magic-T

This section presents a dual-polarization monopulse feed based on the GW technology. Firstly, two planar Magic-T structures are designed, and then these Magic-T structures are utilized to construct a monopulse comparator, resulting in the design of the antenna.

Two types of planar magic-Ts

The planar Magic-T is an excellent choice for the monopulse comparator due to its stable performance and compact size. Fig. 2.1(a) illustrates the geometry of the proposed first type of planar Magic-T. It consists of three RGWs and one E-plane GGW. When the $\text{port}_{1\text{f}}$ is excited, equal-amplitude signals with 0° phase difference can be obtained at the $\text{port}_{3\text{f}}$ and $\text{port}_{4\text{f}}$, respectively. When the $\text{port}_{2\text{f}}$ is excited, equal-amplitude signals with 180° phase difference can be obtained at the $\text{port}_{3\text{f}}$ and $\text{port}_{4\text{f}}$, respectively. Fig. 2.1(b) illustrates the geometry of the proposed second type of planar Magic-T, which comprises three E-plane GGWs and one RGW. Its operation principle is similar to the first type of Magic-T.

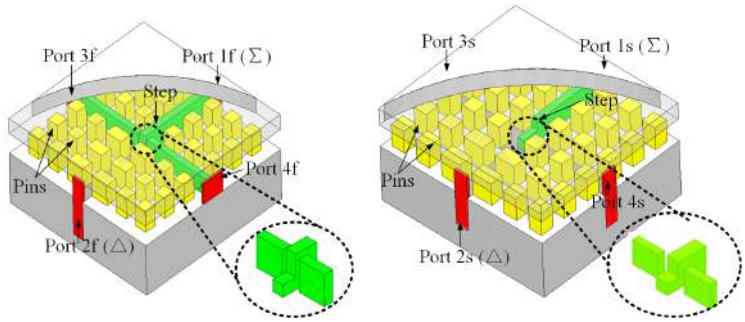

(a) 3(RGW)+(E-GGW) Magic-T. (b) 3(E-GGW)+(RGW) Magic-T.

Figure 2.1: Geometries of two types of Magic-Ts.

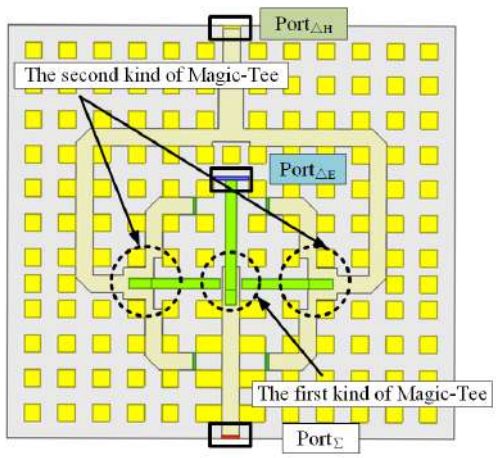

Figure 2.2: Proposed monopulse comparator.

Monopulse comparator

The monopulse comparator is realized using the combination of the first type of Magic-T, the second type of Magic-T, and the E-plane T-junction. The geometry of the comparator is shown in Fig. 2.2. The monopulse comparator features three ports: sum port $\text{Port}_{\sum}$, E-plane difference port $\text{Port}_{\Delta\text{E}}$, and H-plane difference port $\text{Port}_{\Delta\text{H}}$.

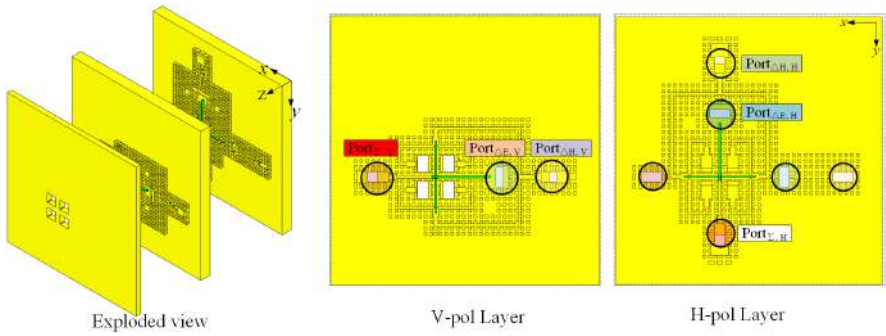

Figure 2.3: Whole geometry of dual-polarized monopulse feed.

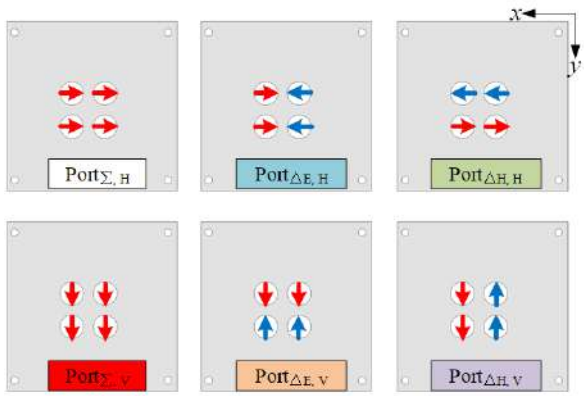

Figure 2.4: Electric field direction for different input ports.

Dual-polarized monopulse feed

This feed structure consists of three layers: 1) the radiating layer, 2) the V-pol layer, and 3) the H-pol layer. The radiating layer is a 2 × 2 square array, with the V-pol and H-pol layers employing a structure similar to an orthogonal mode transducer (OMT) to achieve horizontal polarization and vertical polarization. Due to the utilization of GW technology, the three layers of the monopulse feed can be easily assembled using a few screws. Upon excitation of the ports, the corresponding electric field directions within the radiating aperture can be obtained according to the characteristics of the

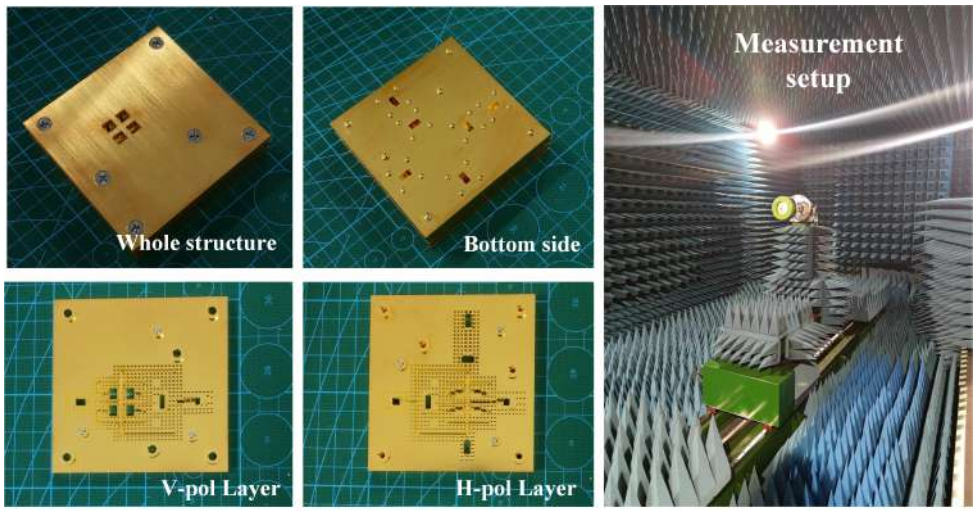

Figure 2.5: Prototype and measurement setup of dual-pol monopulse feed.

monopulse comparator, as depicted in Fig, 2.4, resulting in the SUM and DIFF patterns in dual polarizations.

The fabricated monopulse antenna, as shown in Fig. 2.5, has dimensions of $75 \times 75 \times 20$ mm^3. Measurement results demonstrate that this antenna exhibits excellent monopulse performance across the entire E-plane and H-plane planes throughout the frequency band. For further details, please refer to **Paper B**.

2.3 Monopulse Antenna Based on Phase Shifter

This section presents a monopulse antenna design based on a 3 dB coupler and a 90° phase shifter. Although the previous section discussed designs based on the Magic-T structure, the fabrication of ridges faces many challenges in high-frequency applications. To overcome this issue, this section proposes a more reliable solution. Initially, we introduce a design for a wideband monopulse antenna based on the E-plane Groove Gap Waveguide (GGW). Subsequently, we explore an innovative approach that achieves DIFF beam tracking through phase compensation.

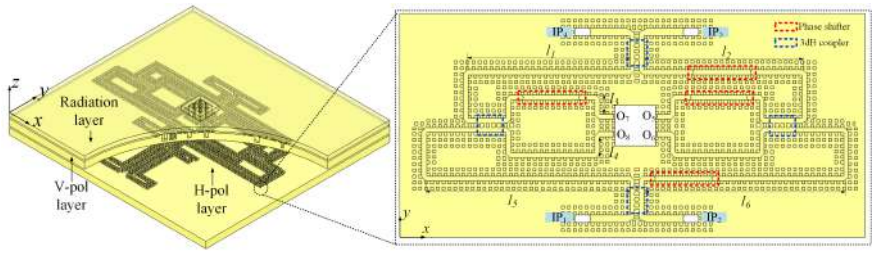

Figure 2.6: Geometry of the monopulse antenna and the feeding network.

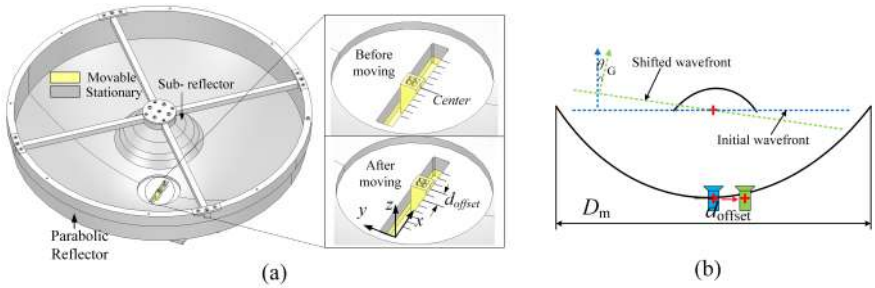

Figure 2.7: Geometric of the reflector antenna. (a) Actual structure. (b) Line model.

Monopulse antenna

The full geometric configuration of the monopulse antenna is depicted in Fig. 2.6. The bottom layer, known as the H-pol layer, is specifically engineered to generate a horizontally polarized feed network. The middle layer, referred to as the V-pol layer, is responsible for establishing a vertically polarized feed network. The top layer comprises a 2 × 2 array of radiating ports, serving to transform the amplitude and phase from the feed network into SUM and DIFF beams. The antenna's six input ports are situated at the base of the structure (WR12).

One of the challenges faced by such antennas is that, due to the dispersion effect of the waveguide, the phase shifter can only achieve a stable phase difference in a narrow band. However, with the in-depth study of wideband phase shifters [47], this issue has been overcome. The working principle of the wideband phase shifter is to keep the phase shift almost constant within

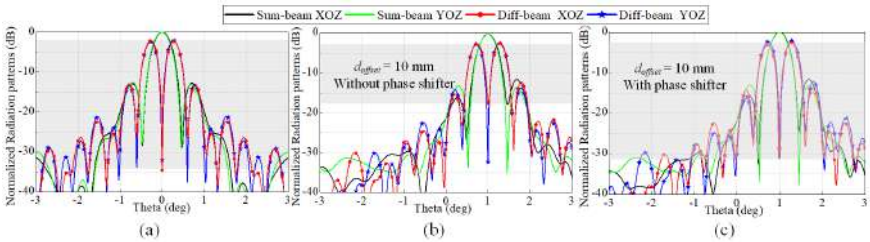

Figure 2.8: Radiation patterns. (a) Central position. (b) After movement without phase shifter. (c) After movement with phase shifter.

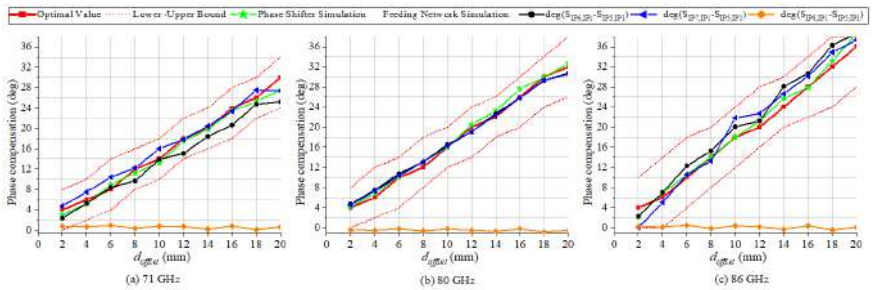

Figure 2.9: Phase curve

a wide frequency band by properly combining two different structures with opposite trends of phase and frequency change curves. This study employs a classic simple structure: delay lines and equal-length unequal-width phase shifters, achieving a 90° phase difference. The top view of the feed network, shown on the right side of Fig. 2.6, includes four 3dB couplers (within the blue dashed line) and four 90° phase shifters (within the red dashed line), where the parameters meet $l_2 - l_1 = l_6 - l_5 = 2(l_4 - l_3) = \triangle l_p = 0.68$ mm.

Tracking principle

Fig. 2.7(a) illustrates the configuration of a Gregorian reflector with a diameter of 0.6 m, which is specially designed with a circular hole with a diameter of 90 mm at the center of the main reflector, providing necessary space for the feed's displacement. When the phase center of the feed is precisely aligned with the focal point of the reflector, as shown by the blue horn in Fig. 2.7(b),

the beam can be directly targeted at boresight. The null depth of the Diff beam can reach 35 dB, as demonstrated in the simulation given in Fig. 2.8(a). As discussed in Chapter chapter 1.3, minor changes in the position of the feed may result in beam deviation, exemplified by the SUM beam in Fig. 2.8(b). For the Diff beam, due to the high sensitivity of the null depth to the phase, any asymmetry caused by slight movement of the feed will significantly deteriorate the null depth. For instance, in Fig. 2.8(b), with just a 10 mm shift of the feed, the null depth of the DIFF beam drastically drops to 15 dB, severely undermining the antenna's tracking ability.

Considering the null depth deterioration of the Diff beam is mainly caused by phase imbalance due to structural asymmetry, this section proposes a phase compensation method based on phase shifters to improve this imbalance. In the initial state of Diff beam formation, the expected phase difference is $\phi_0 = 180°$. This study comprehensively applies GRASP, CST, and MATLAB for joint optimization with the core goal of precise phase adjustment to achieve the most ideal null depth effect. This optimization algorithm is applied at different frequencies, as shown in Fig. 2.9, where the optimal phase differences at 71/80/86GHz are marked with a red solid line. Since phase shifters cannot fully meet the requirements precisely, an acceptable phase error range is defined based on the minimum null depth threshold (20 dB). The red dashed line in Fig. 2.9 represents this limit, and the phase lying between them ensures a null depth exceeding 20 dB when combined with the reflector.

Reconfigurable phase shifter based on gap waveguide

To meet the aforementioned requirements, three types of phase shifters are designed, as shown in Fig. 2.10. These are named length phase shifter, slow-wave phase shifter, and width-variation phase shifter, respectively. They alter the phase by changing the length, slow-wave length, and width respectively. To achieve the required slope, this study combines the slow-wave phase shifter and width-variation phase shifter to realize the final phase shift. The results of the phase shift of the final phase shifter are given in Fig. 2.9, represented as a green solid curve, showing that they all fall within the phase error interval. For further details, please refer to **Paper A and Paper C**.

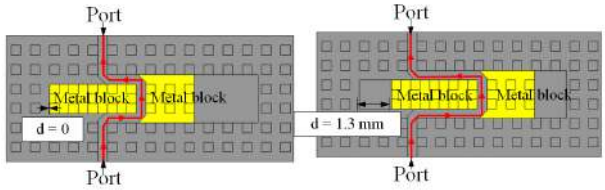

(a) Length phase shifter.

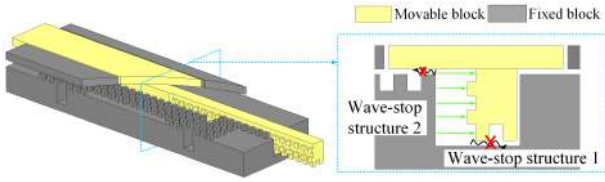

(b) Slow-wave phase shifter.

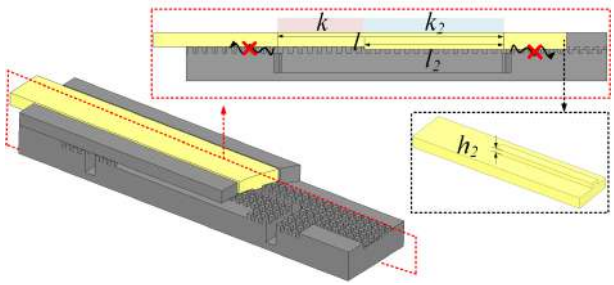

(c) Width-variation phase shifter.

Figure 2.10: Geometries of phase shifter.

Whole antenna

To realize a compact monopulse feed, this study aims to effectively integrate the reconfigurable phase shifter with a monopulse antenna. The main challenge is the dual-pol characteristic of the antenna, requiring simultaneous phase adjustment of the radiation ports in both V-pol and H-pol layers. Although this goal can be achieved by using two independent phase shifters (located in the V-pol and H-pol layers respectively), this method would result in increased cost and structural complexity, thus limiting its effectiveness.

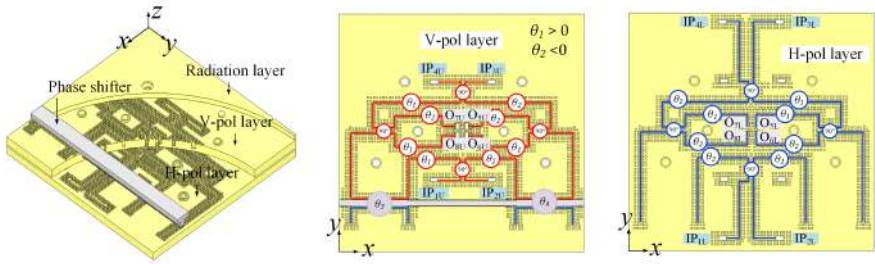

Figure 2.11: Geometries of monopulse antenna. (a) Exploded view. (b) Top view of V-pol layer. (c) Top view of H-pol layer.

	Phase(O_{5U})	Phase(O_{6U})	Phase(O_{7U})	Phase(O_{8U})	Phase(O_{5U})- Phase(O_{6U})	Phase(O_{8U})- Phase(O_{7U}) +180°	Phase(O_{7U})- Phase(O_{8U}) +180°		
IP_{1U}	$180° + 2\theta_2 + \theta_4$	$90° + \theta_2 + \theta_1 + \theta_4$	$\theta_1 + 90° + \theta_2 + \theta_3$	$2\theta_1 + \theta_3$	0	$180° + \theta_4 - \theta_3$	$180° + \theta_4 - \theta_3$		$Port_{\Delta H,V}$
IP_{2U}	$2\theta_2 + 90° + \theta_4$	$\theta_2 + \theta_1 + \theta_4$	$180° + \theta_1 + \theta_2 + \theta_3$	$90° + 2\theta_1 + \theta_3$	0	$\theta_4 - \theta_3$	$\theta_4 - \theta_3$		$Port_{\Sigma,V}$
IP_{3U}	$2\theta_2$	$\theta_2 + 90° + \theta_1$	$90° + \theta_1 + \theta_2$	$180° + 2\theta_1$	-180°	0	-180°		$Port_{\Delta E,V}$
IP_{4U}	$90° + 2\theta_2$	$180° + \theta_2 + \theta_1$	$\theta_1 + \theta_2$	$90° + 2\theta_1$	-180°	180°	0°		Load

(a)

	Phase(O_{5L})	Phase(O_{6L})	Phase(O_{7L})	Phase(O_{8L})	Phase(O_{5L})- Phase(O_{6L}) +180°	Phase(O_{7L})- Phase(O_{7L})	Phase(O_{5L})- Phase(O_{8L}) +180°		
IP_{1L}	$180° + 2\theta_1 + \theta_4$	$90° + \theta_1 + \theta_2 + \theta_4$	$\theta_1 + 90° + \theta_2 + \theta_3$	$2\theta_2 + \theta_3$	0	$180° + \theta_4 - \theta_3$	$180° + \theta_4 - \theta_3$		$Port_{\Delta E,H}$
IP_{2L}	$2\theta_1 + 90° + \theta_4$	$\theta_1 + \theta_2 + \theta_4$	$180° + \theta_1 + \theta_2 + \theta_3$	$90° + 2\theta_2 + \theta_3$	0	$\theta_4 - \theta_3$	$\theta_4 - \theta_3$		$Port_{\Sigma,H}$
IP_{3L}	$2\theta_1$	$\theta_1 + 90° + \theta_2$	$90° + \theta_2 + \theta_1$	$180° + 2\theta_2$	180°	0	180°		$Port_{\Delta H,H}$
IP_{4L}	$90° + 2\theta_1$	$180° + \theta_1 + \theta_2$	$\theta_1 + \theta_2$	$90° + 2\theta_2$	180°	180°	0°		Load

(b)

Figure 2.12: Phase analysis. (a) V-pol layer. (b) H-pol layer

Therefore, a transition structure is chosen to introduce the H-pol layer into the V-pol layer, as shown in Figure 2.11(a). Figs. 2.11 (b),(c) shows the top views of the V-pol and H-pol layers, while Fig. 2.12 presents the phase analysis, where the red and blue lines respectively represent the direction of energy transmission. This feed network satisfies two key requirements: 1. When the phase shifter is at its initial position, the V-pol and H-pol layers respectively

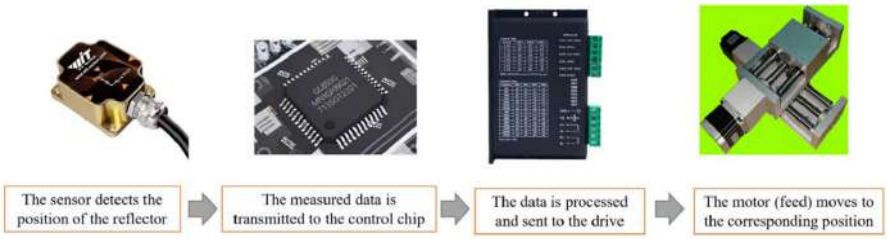

Figure 2.13: Tracking system.

generate one SUM beam and two DIFF beams; 2. When the phase shifter moves along the x-axis, it correspondingly changes the phase of the DIFF beam in the X0Z plane, while the phase of the DIFF beam in the YOZ plane remains unchanged. Fig. 2.9 shows the output phase of the phase shifter, with all phases within the error interval. Lastly, Fig. 2.8(c) displays the radiation direction graph after the feed moves 10 mm, showing improvement in the DIFF beam, better than 30 dB.

2.4 Tracking System

In tracking systems, we utilize angle sensors to precisely perceive the real-time position of the reflector, as shown in Fig. 2.13. These sensors boast an accuracy of up to 0.1°, enabling them to accurately capture variations in position, angle, and direction, thus providing a continuous and reliable stream of positional information to the system. The data from the sensors is transmitted to the control chip. In the event that the position data deviates from the preset values, the control chip swiftly analyzes the information provided by the sensors and formulates a course of action. It promptly sends the corresponding instructions to the driver system. These motors execute movements based on the instructions provided by the control chip. Throughout this process, the system continually receives real-time feedback from the sensors. This allows for timely adjustments and corrections if necessary, ensuring the maintenance of accurate and stable positioning. For detailed design, please refer to **Paper H**.

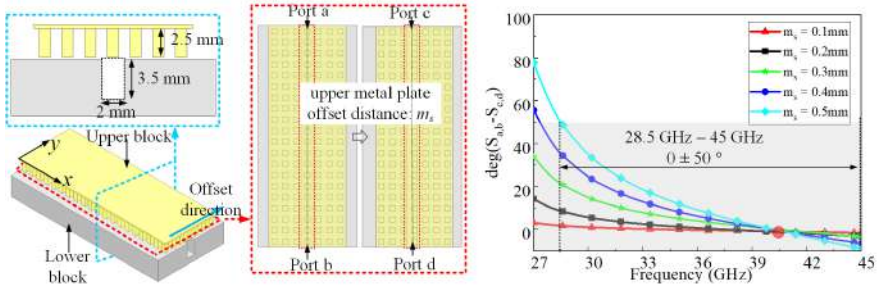

(a) Standard distributed pin structure

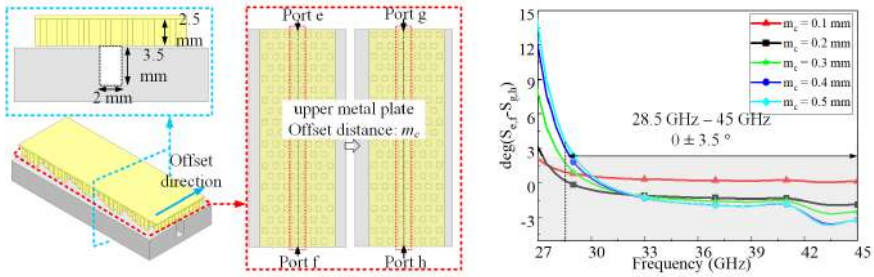

(b) Non-collinear pattern distributed pin structure.

Figure 2.14: Geometries of two kinds of distributed pin structure.

2.5 Pin Distribution Pattern

In the aforementioned designs, we identified that there are still two primary issues with GW in the design process: 1) Groove of the GGW is embedded in the pin bed, which means that any bend in the groove will affect the design of the pin. 2) For complex structures, the simulation and optimization speed in the simulation software CST or HFSS will be slower than the traditional metal waveguide, a problem that becomes more pronounced with electrically larger models. In fact, to overcome these manufacturing challenges, researchers have extensively explored various pin configurations [48]–[51]. A novel type of Half-Mode Gap Waveguide (HM-GGW) was introduced in [50] for rapid prototyping based on GW technology. The HM-GGW does effectively reduce the design time and cost, but some performance, such as the

phase shifts for a device, can be extremely sensitive to the pin position, which for some cases demands on very accurate alignment between the upper and the lower plates in HM-GGW, as a misalignment can lead to erroneous phase distributions. This in turn may cause the manufacture cost increase and cancel out the benefit from applying HM-GGW. To alleviate the misalignment problem, we propose a new pin structure for the upper plate in HM-GGW: pattern distributed pin structure. Two designs of the pattern distributed pin structures, a non-collinear pattern pin structure and a rotated pattern pin structure are presented to show the flexibility of the pattern distributed pin structure and its stability of the performance to misalignments between the upper and the lower

The primary principle of this approach is to use more complex pin configurations to reduce the sensitivity of the waveguide to pin placement. For reference, Fig. 2.14(a) illustrates the standard uniformly distributed pin structure in a straight HM-GGW. We explored the scenario where the upper block is offset along the y-axis, leading to misalignment (blue solid line arrow in Fig. 2.14(a)). Using CST simulations, we investigated the phase variation of the transmission coefficient S_{21} under different offset values (m_s), as shown in Fig. 2.14(a). It can be observed that misalignment has minimal impact on the amplitude of the reflection and transmission coefficients, but significantly affects the phase of the transmission coefficient. For instance, when the upper metal block is offset by 0.5 mm, the phase change is approximately 50°. This phenomenon arises due to the strong influence of the pin positions above the HM-GGW on the field distribution within it, leading to phase variations in the transmission coefficient of the HM-GGW.

To mitigate these phase variations, an idea is to use a patterned distributed pin structure, minimizing the total impact of pin misalignment on the phase of the transmission coefficient and rendering it negligible. Thus, a non-collinear distributed pin structure is proposed for the straight HM-GGW, as depicted in Fig. 2.14(b). The results demonstrate that the non-collinear pin structure exhibits more stable performance compared to the standard uniform pin structure, mitigating the effects of misalignment: the phase change reduces from 50° for the standard pin distribution to 3.5° for the non-collinear pin distribution. The working principle of the non-collinear patterned pin structure is such that, regardless of misalignment, the pins are positioned at different locations above the HM-GGW. As a result, the impact of misalignment can

be negligible, avoiding the scenario in the standard uniformly distributed pin structure where all pins are biased in one direction due to misalignment. For detailed design, please refer to **Paper D**.

2.6 Summary and Conclusion

This chapter begins by introducing the design of a monopulse feed based on the Magic-T, encompassing the creation of two compact planar Magic-T structures. Secondly, the chapter proposes a monopulse feed antenna based on the phase shifter and the coupler, achieving tracking of DIFF beams through phase compensation methods. In addition, three unique compact, low-loss, reconfigurable phase shifters based on GW technology were individually designed. Lastly, a novel concept of pin distribution pattern is introduced to address the phase variations caused by misalignment in the HM-GGW. This also enhances the versatility of the HM-GGW.

CHAPTER 3

Antenna System with Automatic Beam Tracking

3.1 Antenna Design Requirements

In addition to the antenna's beam steering functionality mentioned in **Chapter 1.3**, the antenna's design entails other significant requirements, as shown in Table. 3.1. When achieving beam steering by deflecting the feed antenna away from the sub-reflector focus, it is imperative to ensure the connection interface with other components of the radio system, such as the T/R module, remains stationary. This approach aims to guarantee connection reliability, reduce the likelihood of faults, and, when operating at mmWave frequencies, the use of coaxial cables can prevent bending, thereby ensuring dependable signal transmission. However, to achieve this goal, relative movement within the waveguide is inevitable. Therefore, there must be a gap between the moving and stationary parts. At mmWave frequencies, even small gaps can lead to significant energy leakage and detrimental resonances, severely impacting antenna performance. For our research context, a gap of 100 μm must be maintained between the movable and fixed blocks. This numerical value has been verified through mechanical experiments to ensure smooth motion within reasonable manufacturing tolerances.

Table 3.1: Proposed specifications for beam steering antenna.

Required properties	Target value
Polarizations	Dual LP
Frequency	71-86 GHz
Radiation pattern	Low cross-polarization Complies with ETSI Class 3
Gain	approximately 50 dBi
Beam steering	Ability to steer beam by at least ± 2 deg
Others	A stationary interface between the moving feed and the rest of the system & Instantaneous beam tracking function

Within this chapter, we have adopted GW technology to maintain the required gap while effectively preventing wave leakage and undesired resonances. The operational principles of GW technology were introduced in **Chapter 1.4**. Here, we utilize the non-contact characteristics of GW technology to design a novel movable feed structure. This innovation holds the potential to provide a more sustainable solution for antenna design reliability and performance enhancement.

3.2 Antenna System with Automatic 1D Beam Tracking Capability

Non-contact GW devices

Prior to antenna design, we initially developed a series of non-contact devices. Non-contact devices refer to components composed of several metal blocks that do not require electrical contact between them as long as the gaps between these metal blocks do not exceed the maximum allowable distance. Thus, relative movement between different parts is feasible.

This study introduces three types of reconfigurable transmission lines (TLs): a sheath rectangular waveguide, a movable rectangular waveguide, and a universal-joint circular waveguide, as depicted in Fig. 3.1. These configurations aim to extend the application of GW technology to the field of mechanical reconfigurability. Utilizing GW technology, these three reconfigurable TLs

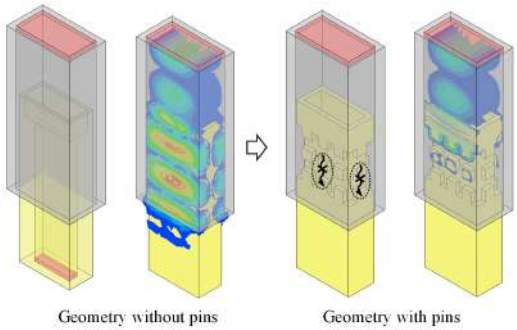

(a) Sheath rectangular waveguide transmission line

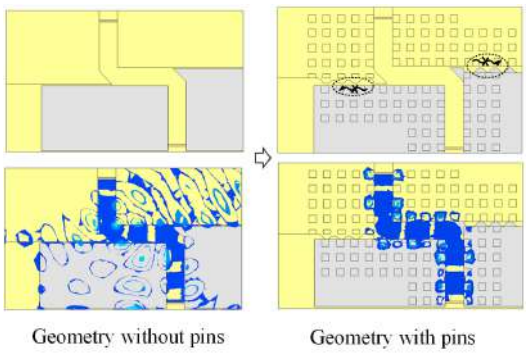

(b) Movable rectangular waveguide transmission line

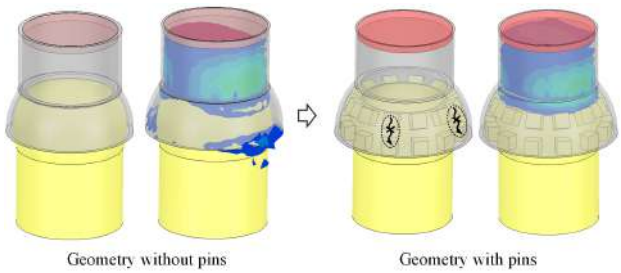

(c) Universal-joint circular waveguide transmission Line

Figure 3.1: Geometry of transmission line.

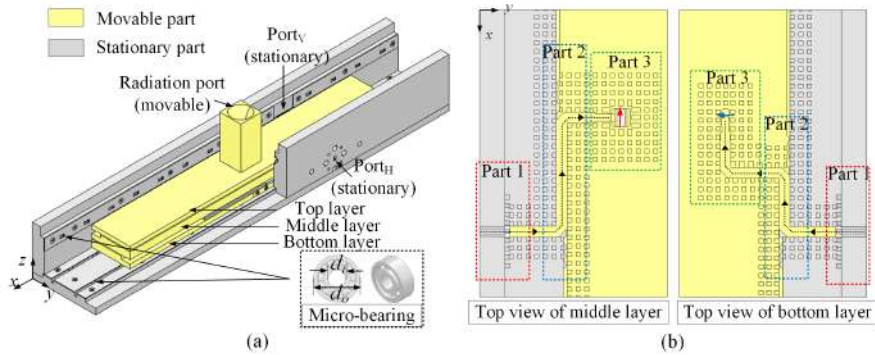

Figure 3.2: Geometry of the movable GW feed. (a) The overall structure (part of the stationary plates are hidden for easy viewing). (b) Top view of different layers.

enable the movement of waveguide ports through shielded, displacement, and rotation mechanisms while minimizing leakage during electromagnetic wave propagation. For detailed design, please refer to **Paper E**.

Antenna design with 1D beam steering capability

Based on the aforementioned non-contact GW devices, we have designed a movable GW feed, whose geometry is illustrated in Fig. 3.2. This movable section (in yellow) consists of three layers: the top layer features dual-polarized horns, the middle layer employs a polarized feeding network, and the bottom layer is equipped with another polarized feeding network. Due to the properties of GW, these three layers can be easily assembled using several screws without wave leakage. In the fixed section (in gray), there are two stationary ports for connecting to the radio system: the vertical polarization port Port_V and the horizontal polarization port Port_H. The movable section can slide along the x-axis, while the connection ports remain fixed. Fig. 3.2(b) depicts a top view of the middle and bottom layers, each composed of three parts. The Part1 and Part2 are based on the non-contact transmission line discussed in the previous section, and the Part3 employs orthomode transducer to achieve dual-polarization.

To validate the design of the movable GW feed, a prototype was fabricated

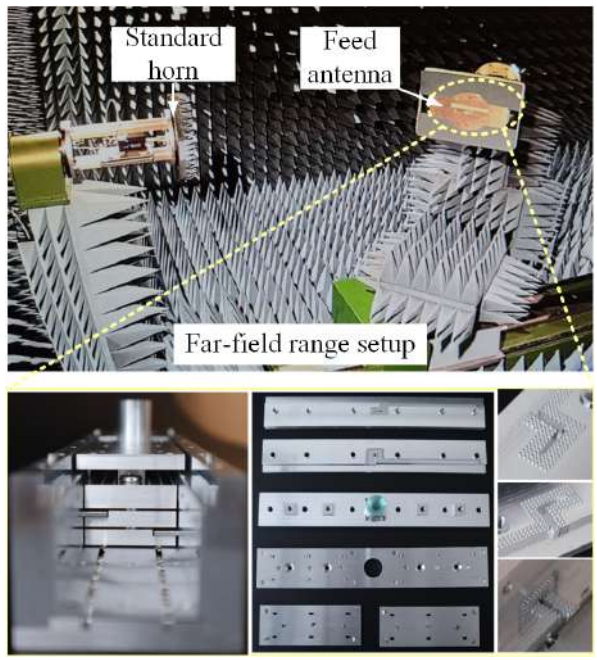

keyiya

Figure 3.3: Prototype and measurement setup of the movable feed.

using CNC machining technology, with a total weight of approximately 2 kg. Regarding electrical characteristics, the measured reflection coefficient of the entire feed was below −10 dB. Simulation and measured gains exhibited consistency, indicating minimal wave leakage within the prototype. Concerning the mechanical properties, very low frictional resistance is exhibited during the sliding process. These measurement results demonstrate that the proposed feed exhibits excellent performance across the entire frequency range and under both polarizations.

The fabrication of the reflector has been completed, as depicted in Fig. 3.4. The radiation characteristics was conducted using a compact range setup. The measurement results, as depicted in Fig. 3.5, showcase the simulated and measured radiation patterns for both H-pol and V-pol in the E-plane and H-plane. A detailed radiation pattern within the range of $\theta \in$ [-5°, 5°] is shown in the top-left corner of the figure. It is evident that the first sidelobe

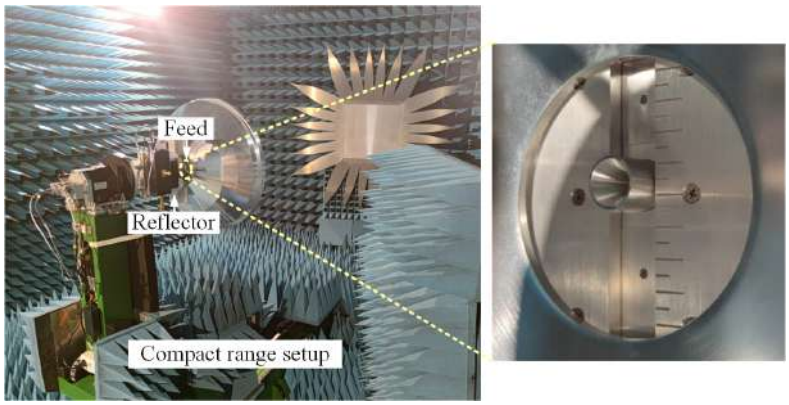

Figure 3.4: Prototype and measurement setup of reflector antenna.

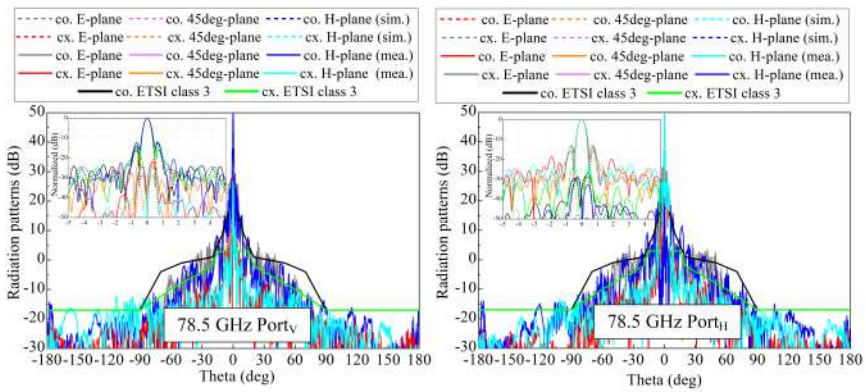

Figure 3.5: Simulated and measured radiation patterns of the proposed reflector antenna.

level remains below −13 dB, while the level of cross-polarization is below −20 dB. Additionally, Fig. 3.6 displays the simulation and measurement outcomes for beam steering. Within a 2-deg range of movement, a linear relationship is observed between the displacement distance and deflection angle, with a decrease in gain of less than 1 dB. The design detail and results analysis is presented in **Paper G**.

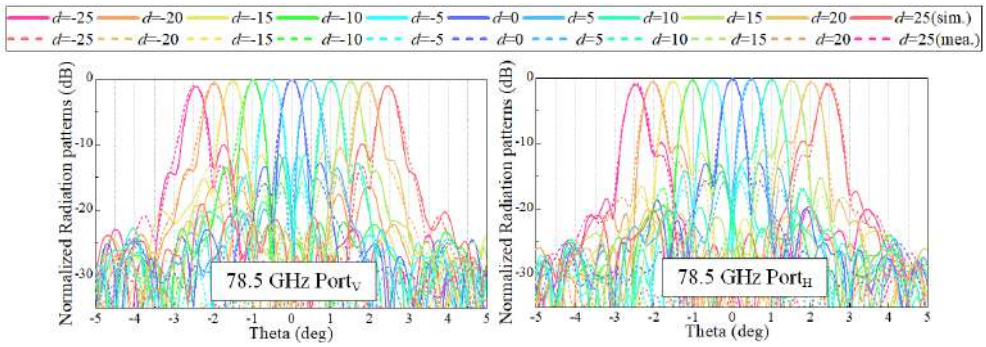

Figure 3.6: Simulated and measured beam steering of the proposed reflector antenna. (Units: mm)

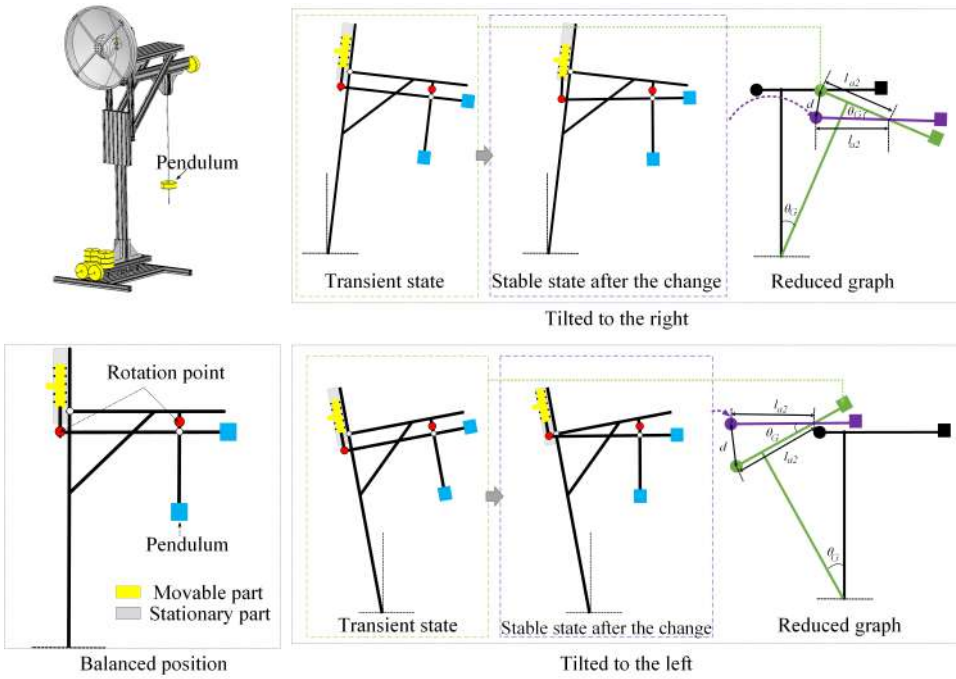

Figure 3.7: Gravity-driven system.

Gravity-driven System

In the **Chapter 2.4**, we employed sensors and the electric motor system to achieve beam tracking. In this chapter, we introduce a novel automated tracking system that utilizes the force of gravity to compensate for beam oscillations caused by mast swaying. The gravity-driven system for movable feed is illustrated in Fig. 3.7. In this solution, a large "pendulum" is maintained in vertical balance by utilizing the restorative force generated during mast swinging. Subsequently, a balancing system is applied to the pivot of the pendulum to generate the driving force that shifts the feed from the apex to the correct position. Thus, the mast is rotated at a negative angle θ to counteract the mast's swinging angle θ, thereby maintaining the beam direction horizontal during mast oscillations.

Measurement verification indicates that the gravity-driven system is well-suited for slow sway, with precise displacement positions corresponding to the respective oscillation angles. This technology offers advantages such as low cost, real-time response, and energy efficiency, making it more environmentally friendly. The design detail and results analysis is presented in **Paper G** and **Paper H**.

3.3 Antenna System with Automatic 2D Beam Tracking Capability

Chapter 1.3 identifies three modes of mast oscillation induced by external factors: elevation sway, transverse sway, and azimuth sway. In **Chapter 3.2**, the design of a 1D beam-tracking antenna specifically addresses elevation sway. This section expands upon that foundation, presenting a design that accommodates both elevation and azimuth sway, thereby establishing a 2D beam-tracking antenna system. Additionally, we have formulated a more robust gravity compensation system.

Antenna design with 2D beam steering capability

To achieve the effect of stationary port and 2D motion of the radiating part, we designed a structure as shown in Fig. 3.8. The underlying principle of this design is similar to that presented in **Chapter 3.2**, with the distinction that in

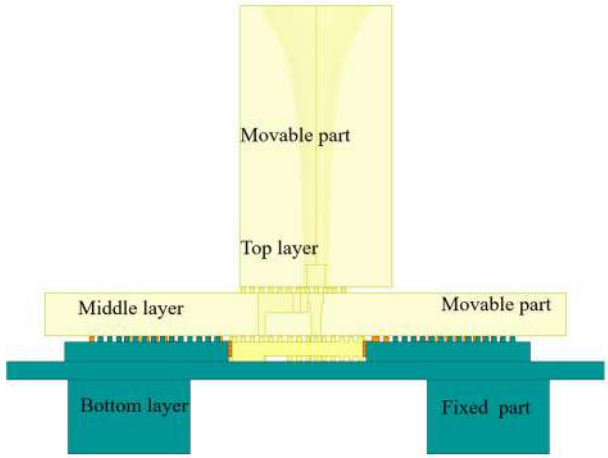

(a) Side view

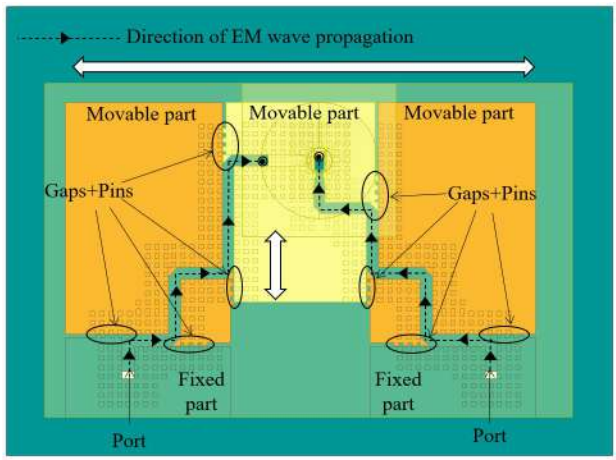

(b) Bottom view

Figure 3.8: Geometry of 2D movable GW feed.

this particular design, the middle and top layers are movable while the bottom layer remains fixed. When only the middle metal block (yellow portion) moves along the vertical arrow direction (as seen in the bottom view), the radiation

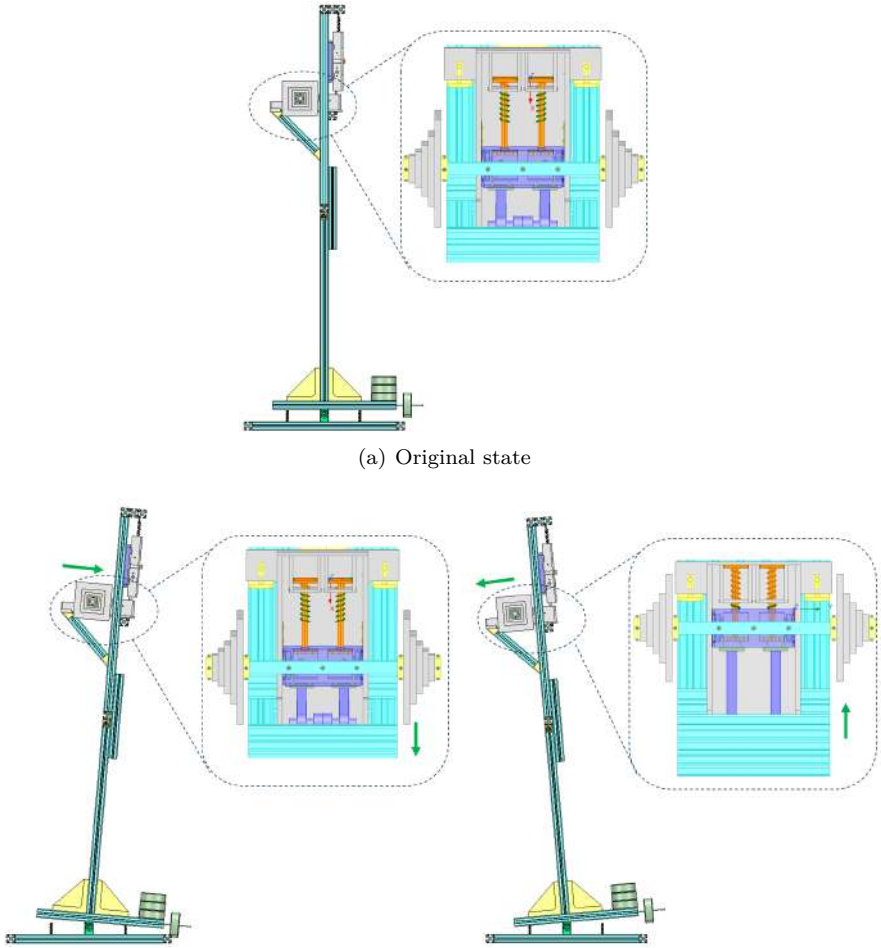

(a) Original state

(b) Lean to the left

(c) Lean to the right

Figure 3.9: Gravity-driven spring system.

aperture moves vertically. However, when all three metal blocks (yellow and orange portions) move simultaneously along the horizontal arrow direction, the radiation aperture moves horizontally, thus achieving the functionality of a 2D movable GW feed.

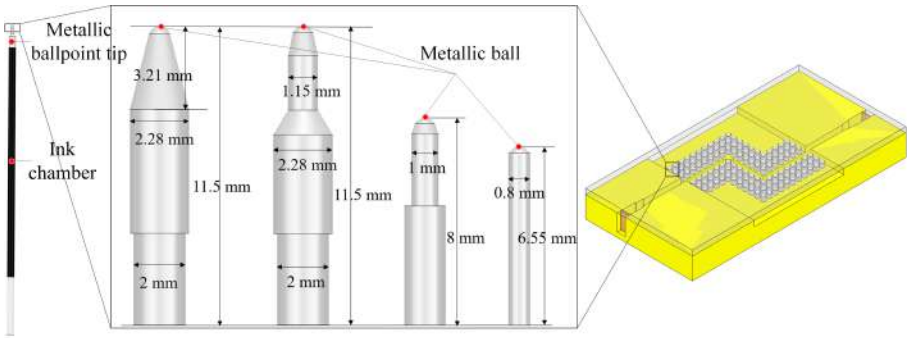

Figure 3.10: Geometries of the ball-pen and the double 90-deg bent ball-pen GW

Gravity-driven spring system

To avoid resonance during rapid changes, we have made improvements to this aspect by replacing the original gravity-driven system with a gravity-driven spring system. Fig. 3.9 illustrates the basic configuration of this solution. Preliminary simulations indicate that when the mast swings to the left (or right) by an angle of θ, the direction of the beam will shift upwards (or downwards) relative to the horizontal direction by an angle of θ. Subsequently, the feed and weight load will slide downward (or upward) due to gravity. By employing an appropriate spring system, when the forces of the spring and gravity balance each other, the feed will move to the correct position, causing the beam direction to shift from a downward (or upward) angle of θ to a horizontal position, thus maintaining the stability of the beam direction.

3.4 Low-cost Ball-pen GW with Nearly Zero Friction for Sliding Movements

To minimize friction during the sliding process of the aforementioned antenna, this section introduces a easy-to-manufacture GW using the ballpoint of commercially available, low-cost pens, termed the "Ball-pen GW", as shown in Fig. 3.10. The proposed Ball-pen GW consists of a perforated bottom metal plate into which the tip of a ball-pen is inserted, and a flat top plate. Unlike other non-contact GWs with pin-bed structures attained through milling, the

Ball-pen GW is realized simply by drilling holes in the bottom plate for the insertion of the ball-pen tips, facilitating electromagnetic band-gap properties at a lower cost. A crucial advantage of the Ball-pen GW is the employment of the ball from the pen's tip to achieve smooth, low-friction sliding motion, beneficial for mechanical reconfiguration. This approach not only simplifies the manufacturing process but also significantly reduces costs associated with traditional methods, all the while maintaining efficient performance for the antenna's mechanical restructuring. For detailed design, please refer to **Paper F**.

3.5 Summary and Conclusion

This chapter initially presents three distinct reconfigurable TLs for the advancement of reconfigurable antennas: the Sheath RWTL, the Movable RWTL, and the Universal-joint CWTL. These TLs enable precise manipulation of the position and direction of the TLs through sheathing, displacement, and rotational actions. Subsequently, based on these TLs, two types of dual-polarized, low-loss, and cost-effective movable GW feeds are designed. These feeds are paired with Gregorian reflector antenna to accomplish ultra-high-gain antennas with 1D and 2D beam steering capabilities. Following this, gravity-driven systems and gravity-driven spring systems are devised to achieve 1D and 2D beam tracking. Lastly, the Ball-pen GW is proposed to reduce friction during the antenna's movement process, optimizing performance during reconfigurations.

CHAPTER 4

Summary of included papers

This chapter provides a summary of the included papers.

4.1 Paper A

E. Wang, J. Yang, A. U. Zaman
An E-band reconfigurable phase shifter based on gap waveguide
2022 16th European Conference on Antennas and Propagation (EuCAP), Madrid, Spain, Mar. 2022.

In this paper, an E-band reconfigurable phase shifter based on GW technology is designed. Many different phase shifts can be easily achieved by controlling the movable metal blocks. The use of GW technology makes the phase shifter with low loss and prevents wave leakage. Obviously, the proposed phase shifter has good performance, including low loss, simple processing and so on.
Author's Contributions: Design, modeling, EM simulation, manuscript writing.

4.2 Paper B

E. Wang, T. Zhang, A. U. Zaman, T. Emanuelsson, P. Thorsen, S. Agneessens, J. Yang
A compact gap-waveguide dual-polarized Ka-band feed for 50 dBi reflector antennas with tracking function
IEEE Access, vol. 10, pp. 91622-91630, Aug. 2022.

In this paper, a dual-polarized monopulse feed, composed of three contactless plates, has been proposed based on gap waveguide technology with two types of planar GW magic tees to form a monopulse comparator. Due to the separate plates, the manufacture cost has been reduced a lot with a low-loss characteristic, where the assembly tolerance is relatively easy to be guaranteed. The feed has been designed and manufactured. The measurements of the prototype have verified the design of the feed. Finally, the designed feed is used to feed a dual-reflector Cassegraine antenna with the simulations of numerical modeling in GRASP to achieve an ultra-high gain of above 50 dBi with 2D tracking functions. The proposed antenna is aiming to be used in 5G mmWave backhauling systems.
Author's Contributions: Design, modeling, EM simulation, measurements, manuscript writing.

4.3 Paper C

E. Wang, S. Agneessens, A. U. Zaman, H. Karlsson, Z. Yan, J. Yang
E-band low-loss reconfigurable phase shifters
IEEE Microwave and Wireless Technology Letters, vol. 33, no. 7, pp. 999-1002, Mar. 2023.

Two E-band low-loss mechanically reconfigurable phase shifters based on GW mechanical motion technique have been proposed, designed, and verified. Due to the use of the quasi-PEC-AMC structure, no wave leakage and undesired resonances appear throughout the E-band. The insertion losses are below 0.4 dB and the reflection coefficients below -13 dB.
Author's Contributions: Design, modeling, EM simulation, measurements, manuscript writing.

4.4 Paper D

E. Wang, A. U. Zaman, Z. Yan, J. Yang
Pattern distributed pins in half-mode groove gap waveguide for stable performance and low cost
2023 17th European Conference on Antennas and Propagation (EuCAP), Florence, Italy, Mar. 2023 .

In this paper, a new concept of pattern distributed pin structure is proposed to improve the stability of the phase performance when there is a misalignment in a half-mode groove gap waveguide (HM-GGW) and therefore reduce the manufacture cost. To demonstrate the advantages of the pattern distributed pin structure, a non-collinear pin pattern and a rotated pin pattern are proposed and applied to a straight HM-GGW and a 90-deg bend HM-GGW. The dispersion diagram and simulation results show that the pattern distributed pin structure has a similar stop-band characteristics as the standard pin structure with much less sensitivity to misalignments between the upper pins and the lower wave-guiding structure. By applying a proper pattern distributed pin structure, a larger flexibility is obtained in design of GW devices and the manufacture cost can be reduced significantly.
Author's Contributions: Design, modeling, EM simulation, manuscript writing.

4.5 Paper E

E. Wang, S. Agneessens, O. Talcoth, C. Bencivenni, A. U. Zaman, J. Yang
Applications of contactless characteristics of gap waveguides in mechanical reconfigurability
2023 International Symposium on Antennas and Propagation (ISAP), Kuala Lumpur, Malaysia, Oct. 2023 .

This paper introduces three distinct reconfigurable TLs for the advancement of reconfigurable antennas: the sheath-RWTL, the Movable-RWTL, and the Universal-joint-CWTL. These TLs enable precise manipulation of the TL's position and orientation through sheathing, displacement and rotational operations. Notably, all three structures incorporate the utilization of GW technology to form a PEC-AMC structure within every gap, effectively suppressing

energy leakage and reducing the loss to a level below 0.3 dB.
Author's Contributions: Design, modeling, EM simulation, manuscript writing.

4.6 Paper F

E. Wang, A. U. Zaman, Z. Yan, J. Yang
Low-cost ball-pen gap waveguide with nearly zero friction for reconfigurable movements
IEEE Microwave and Wireless Technology Letters, vol. 33, no. 11, pp. 1580-1583, Sep. 2023 .

This paper presents a novel easy-to-manufacture ball-pen gap waveguide (GW) by utilizing commercial low-cost ball-pens to have mechanical reconfigurability. The proposed ball-pen GW consists of a perforated bottom metal plate with ball-pens' tips inserted and a flat top plate. Compared with the other non-contact GWs with a bed-of-pins structures obtained by milling, the realization of the new ball-pen GW requires only drilling holes on the bottom plate for inserting ball-pen tips to obtain the electromagnetic band gap property, making it low cost. The more important advantage of the ball-pen GW is to make use of the balls of the ball-pen tips to realize a smooth low-friction sliding movements for the mechanical reconfiguration. For the sake of verification, a double 90° bend of the ball-pen GW has been designed, manufactured, and measured. Both simulated and measured results demonstrate its excellent transmission performance and the movable property.
Author's Contributions: Design, modeling, EM simulation, measurements, manuscript writing.

4.7 Paper G

E. Wang, S. Agneessens, O. Talcoth, L. Manholm, C. Bencivenmi, E. Alfonso, A. Wennergren, H. Stalrud, A. U. Zaman, and J. Yang
A 50 dBi E-band dual-reflector antenna for 5G backhauling with auto-beam-tracking function
Submitted to IEEE Transactions on Antenna and Propagation .

An ultra-high-gain E-band dual-reflector antenna for 5G backhaul with

beam tracking function is proposed in this paper. Beam tracking is achieved by defocussing the feed away from the focus point of the dual reflector system, while keeping the interface with the transmit-receive unit stationary by applying a movable gap-waveguide configuration. The antenna has been prototyped and measured. The measured reflection coefficients remain below -10 dB for both horizontal and vertical polarizations over $71-86$ GHz, almost independent from the offset positions of the feed. The measured radiation patterns agree well with the simulated ones, with a peak gain of about 50 dBi in the band and less than 1 dB gain drop for beam steering within $\pm 2^{\circ}$. Finally, a low-cost and environmentally friendly mechanical tracking system is proposed, prototyped, and tested. Measurements verify that the tracking system functions well for slow sways.
Author's Contributions: Design, modeling, EM simulation, measurements, manuscript writing.

4.8 Paper H

E. Wang, A. Wennergren, H. Stalrud, C. Bencivenmi, E. Alfonso, A. U. Zaman, and J. Yang
Antenna and mechanical co-design for auto-beam-tracking in backhaul systems
Submitted to 18th European Conference on Antennas and Propagation .

This paper addresses the electrical-mechanical co-design challenges of beam alignment in ultra-high-gain antennas due to mast sway by adopting a defocusing strategy for the reflector antenna feed in order to meet the requirements of 5G mmWave backhaul communication systems. Three automatic beam tracking methods have been investigated and evaluated: a sensor-motor-based control method, a gear-driven compensation method by using a secondary mast as a reference, and a gravity-driven pendulum method that leverages gravitational force as the reference. Detailed description of the integrated design approach combining both antenna design and mechanical structure is given in the paper, providing potential platform for further improved system developments.
Author's Contributions: Design, modeling, EM simulation, manuscript writing.

CHAPTER 5

Future Works

While the quest for high capacity is crucial, the robustness of 5G backhaul systems is equally important to ensure stable communication services at all times and under all conditions. To enhance the robustness of backhaul systems, lower frequency bands can be considered. As shown in Fig. 5.1, existing solutions have been designed for both high capacity and robustness, exemplified by a 10-kilometer link aggregation example. Specifically, this example comprises a traditional microwave radio link operating at 18 GHz with a throughput of 1 Gbps and high availability of 99.997%, along with an E-band radio link that offers 10 Gbps throughput (up to 20 Gbps in XPIC configurations) and 99.7% availability (equivalent to 26 hours, 16 minutes and 48 seconds of unavailability per year), as shown in Fig. 5.2.

This link combination seamlessly integrates traditional microwave links in lower frequency bands with high-capacity E-band radio links, providing superior resistance to rain and other atmospheric conditions. This ensures the stable transmission of all priority traffic, while mmWave radio links deliver nearly year-round maximum capacity. Although the E-band antennas contribute to high capacity, the robustness of the link is typically maintained by the more stable lower frequency bands. However, using different aperture sizes

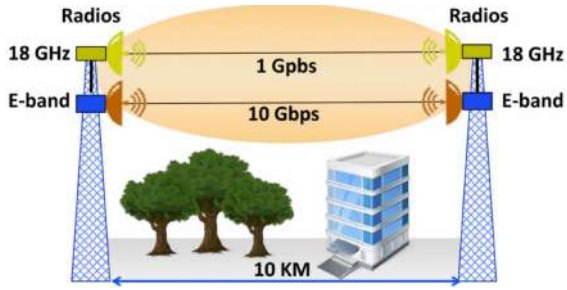

Figure 5.1: Link aggregation (E-band + 18 GHz band). [52]

Radio link	Distance [Km]	Throughput [Gbps]	Rain [mm/h]	Availability
18-GHz	10	1 with XPIC	42	99.997%
E-band	10	10	42	99.7%

E-Band Radio link		Unit
Availability	99.7	%
Rain intensities	42	[mm/h]
Antenna (diameter)	60	[cm]
Transmitted Power	24	[dBm]
Modulation scheme	128 QAM	
Channel bandwidth	2000	[MHz]
Throughput	10	[Gbps]

Figure 5.2: E-band and 18GHz link aggregation in backhauling over 10 km for high capacity and robustness. [52]

(reflectors) for the two frequency bands could pose a considerable burden on societal sustainability. Therefore, there is an urgent need for a solution that employs dual-band antennas with identical aperture sizes to support backhaul systems across both frequency bands, thereby reducing the volume of antennas and masts. So our future goal is to develop a dual-band, high-gain antenna equipped with real-time tracking capabilities to provide consistent, high-capacity, and robust communication services. This will significantly bolster the advancement of 5G backhaul systems and is expected to further propel technological developments in the communication field.

References

[1] S. Chia, M. Gasparroni, and P. Brick, "The next challenge for cellular networks: Backhaul," *IEEE Microw. Mag.*, vol. 10, no. 5, pp. 54–66, 2009.

[2] M. Xiao, S. Mumtaz, Y. Huang, *et al.*, "Millimeter wave communications for future mobile networks," *IEEE J. Sel. Areas Commun.*, vol. 35, no. 9, pp. 1909–1935, 2017.

[3] J. G. Andrews, S. Buzzi, W. Choi, *et al.*, "What will 5g be?" *IEEE J. Sel. Areas Commun.*, vol. 32, no. 6, pp. 1065–1082, 2014.

[4] A. Ghosh, T. A. Thomas, M. C. Cudak, *et al.*, "Millimeter-wave enhanced local area systems: A high-data-rate approach for future wireless networks," *IEEE J. Sel. Areas Commun.*, vol. 32, no. 6, pp. 1152–1163, 2014.

[5] "Enabling smart traffic with advanced traffic control systems," Available: https://www.analog.com/media/en/news-marketing-collateral/product-highlight/enabling-smart-traffic-with-advanced-traffic-control-systems.pdf.

[6] M. Marcus and B. Pattan, "Millimeter wave propagation: Spectrum management implications," *IEEE Microw. Mag.*, vol. 6, no. 2, pp. 54–62, 2005.

[7] J. Du, E. Onaran, D. Chizhik, S. Venkatesan, and R. A. Valenzuela, "Gbps user rates using mmwave relayed backhaul with high-gain antennas," *IEEE J. Sel. Areas Commun.*, vol. 35, no. 6, pp. 1363–1372, 2017.

[8] F. C. Commission *et al.*, "Allocation and service rules for the 71–76 ghz, 81–86 ghz and 92–95 ghz bands," *FCC Memorandum Opinion and Order*, pp. 03–248, 2003.

[9] G. Amendola, L. Boccia, F. Centurelli, *et al.*, "Compact e-band i/q receiver in sige bicmos for 5g backhauling applications," *IEEE Trans. Circuits Syst. II, Exp. Briefs*, vol. 68, no. 9, pp. 3098–3102, 2021.

[10] D. Lockie and D. Peck, "High-data-rate millimeter-wave radios," *IEEE Microw. Mag.*, vol. 10, no. 5, pp. 75–83, 2009.

[11] C. Oestges, B. Clerckx, M. Guillaud, and M. Debbah, "Dual-polarized wireless communications: From propagation models to system performance evaluation," *IEEE Trans. Wirel. Commun.*, vol. 7, no. 10, pp. 4019–4031, 2008.

[12] C. Hendrix, G. Kulon, C. Anderson, and M. Heinze, "Multigigabit transmission through rain in a dual polarization frequency reuse system: An experimental study," *IEEE Trans. Commun.*, vol. 41, no. 12, pp. 1830–1837, 1993.

[13] "Ericsson micrwave outlook 2021," [online]Available: https://www.ericsson.com/en/reports-and-papers/microwave-outlook/reports/2021.

[14] R. Kalimulin, A. Artemenko, R. Maslennikov, J. Putkonen, and J. Salmelin, "Impact of mounting structures twists and sways on point-to-point millimeter-wave backhaul links," *Proc. IEEE Int. Conf. Commun. Workshop (ICCW)*, pp. 19–24, 2015.

[15] Y. Fujino, N. Hamamoto, A. Miura, *et al.*, "Tradeoff study on array-fed reflector antennas for 100-beam-class multibeam communications satellite," in *2010 IEEE Antennas Propag. Soc. Int. Symp.*, 2010, pp. 1–4.

[16] A. Mozharovskiy, A. Artemenko, A. Sevastyanov, V. Ssorin, and R. Maslennikov, "Beam-steerable integrated lens antenna with waveguide feeding system for 71–76/81–86 ghz point-to-point applications," in *10th Eur. Conf. Antennas Propag. (EuCAP)*, 2016, pp. 1–5.

[17] M. Faenzi, G. Minatti, D. González-Ovejero, *et al.*, "Metasurface antennas: New models, applications and realizations," *Scientific reports*, vol. 9, no. 1, p. 10 178, 2019.

[18] J. Hautcoeur, E. Motta Cruz, J. Bartholomew, J. Sarrazin, Y. Mahe, and S. Toutain, "Low-cost printed antenna array built with hybrid feed for urban microwave links," *IET Microw. Antennas Propag.*, vol. 4, no. 9, p. 1320, 2010.

[19] Y. H. Cho, W. J. Byun, and M. S. Song, "High gain metal-only reflectarray antenna composed of multiple rectangular grooves," *IEEE Trans. Antennas Propag.*, vol. 59, no. 12, pp. 4559–4568, 2011.

[20] P. Piksa, S. Zvanovec, and P. Cerny, "Elliptic and hyperbolic dielectric lens antennas in mmwaves," *Radioengineering*, vol. 20, no. 1, pp. 270–275, 2011.

[21] S. K. Karki, J. Ala-Laurinaho, V. Viikari, and R. Valkonen, "Lens antenna design for e-band point-to-point radio links," in *2017 PIERS Spring*, 2017, pp. 1625–1631.

[22] M. Oldoni, M. Stefano, B. Goran, G. L. Solazzi, *et al.*, "A steering antenna for long-reach mmwave X-haul links," *Microwave J.*, vol. 64, pp. 1–2, 2021.

[23] D. Cheng and S. Moseley, "On-axis defocus characteristics of the paraboloidal reflector," *IRE Trans. Antennas Propag.*, vol. 3, no. 4, pp. 214–216, 1955.

[24] S. Rahiminejad, E. Pucci, V. Vassilev, P.-S. Kildal, S. Haasl, and P. Enoksson, "Polymer gap adapter for contactless, robust, and fast measurements at 220–325 ghz," *J. Microelectromech. Syst.*, vol. 25, no. 1, pp. 160–169, 2016.

[25] J. Tayebpour, B. Ahmadi, M. Fallahzadeh, O. Shekoofa, and A. Torabi, "A waveguide switch based on contactless gap waveguide technology," *IEEE Microw. Wireless Compon. Lett.*, vol. 29, no. 12, pp. 771–774, 2019.

[26] D. Sun, Z. Chen, C. Yao, and J. Xu, "Flexible rectangular waveguide based on cylindrical contactless flange," *Electron. Lett.*, vol. 52, no. 25, pp. 2042–2044, 2016.

[27] D. Sun and J. Xu, "Real time rotatable waveguide twist using contactless stacked air-gapped waveguides," *IEEE Microw. Wireless Compon. Lett.*, vol. 27, no. 3, pp. 215–217, 2017.

[28] P.-S. Kildal, E. Alfonso, A. Valero-Nogueira, and E. Rajo-Iglesias, "Local metamaterial-based waveguides in gaps between parallel metal plates," *IEEE Antennas Wireless Propag. Lett.*, vol. 8, pp. 84–87, 2009.

[29] A. Uz Zaman, T. Vukusic, M. Alexanderson, and P.-S. Kildal, "Design of a simple transition from microstrip to ridge gap waveguide suited for mmic and antenna integration," *IEEE Antennas Wireless Propag. Lett.*, vol. 12, pp. 1558–1561, 2013.

[30] E. Pucci, E. Rajo-Iglesias, J.-L. Vázquez-Roy, and P.-S. Kildal, "Planar dual-mode horn array with corporate-feed network in inverted microstrip gap waveguide," *IEEE Trans. Antennas Propag.*, vol. 62, no. 7, pp. 3534–3542, 2014.

[31] A. Vosoogh, P.-S. Kildal, and V. Vassilev, "Wideband and high-gain corporate-fed gap waveguide slot array antenna with etsi class ii radiation pattern in V -band," *IEEE Trans. Antennas Propag.*, vol. 65, no. 4, pp. 1823–1831, 2017.

[32] J. Liu, A. Vosoogh, A. U. Zaman, and J. Yang, "Design and fabrication of a high-gain 60-ghz cavity-backed slot antenna array fed by inverted microstrip gap waveguide," *IEEE Trans. Antennas Propag.*, vol. 65, no. 4, pp. 2117–2122, 2017.

[33] M. Ferrando-Rocher, J. I. Herranz-Herruzo, A. Valero-Nogueira, B. Bernardo-Clemente, A. U. Zaman, and J. Yang, "8×8 Ka -band dual-polarized array antenna based on gap waveguide technology," *IEEE Trans. Antennas Propag.*, vol. 67, no. 7, pp. 4579–4588, 2019.

[34] X. Chen, D. Sun, W. Cui, and Y. He, "A folded contactless waveguide flange for low passive-intermodulation applications," *IEEE Microw. Wireless Compon. Lett.*, vol. 28, no. 10, pp. 864–866, 2018.

[35] U. Nickel, "Overview of generalized monopulse estimation," *IEEE Aerosp. Electron. Syst. Mag.*, vol. 21, no. 6, pp. 27–56, 2006.

[36] A. Vosoogh, A. Haddadi, A. U. Zaman, J. Yang, H. Zirath, and A. A. Kishk, "W -band low-profile monopulse slot array antenna based on gap waveguide corporate-feed network," *IEEE Trans. Antennas Propag.*, vol. 66, no. 12, pp. 6997–7009, 2018.

[37] B. Liu, W. Hong, Z. Kuai, *et al.*, "Substrate integrated waveguide (siw) monopulse slot antenna array," *IEEE Trans. Antennas Propag.*, vol. 57, no. 1, pp. 275–279, 2009.

[38] H. Chu, J.-X. Chen, S. Luo, and Y.-X. Guo, "A millimeter-wave filtering monopulse antenna array based on substrate integrated waveguide technology," *IEEE Trans. Antennas Propag.*, vol. 64, no. 1, pp. 316–321, 2016.

[39] Y. J. Cheng, W. Hong, and K. Wu, "94 ghz substrate integrated monopulse antenna array," *IEEE Trans. Antennas Propag.*, vol. 60, no. 1, pp. 121–129, 2012.

[40] J. Zhu, S. Liao, S. Li, and Q. Xue, "60 ghz substrate-integrated waveguide-based monopulse slot antenna arrays," *IEEE Trans. Antennas Propag.*, vol. 66, no. 9, pp. 4860–4865, 2018.

[41] F. Zhao, Y. J. Cheng, P. F. Kou, and S. S. Yao, "A wideband low-profile monopulse feeder based on silicon micromachining technology for w-band high-resolution system," *IEEE Antennas Wireless Propag. Lett.*, vol. 18, no. 8, pp. 1676–1680, 2019.

[42] Y.-X. Zhang, Y.-C. Jiao, L. Zhang, and J.-X. Wen, "Wideband 2-d monopulse antenna array with higher-order mode substrate integrated waveguide feeding and 3-d printed packaging," *IEEE Trans. Antennas Propag.*, vol. 68, no. 4, pp. 3259–3264, 2020.

[43] Z.-C. Hao, H.-H. Wang, and W. Hong, "A novel planar reconfigurable monopulse antenna for indoor smart wireless access points' application," *IEEE Trans. Antennas Propag.*, vol. 64, no. 4, pp. 1250–1261, 2016.

[44] P. Zheng, G. Q. Zhao, S. H. Xu, F. Yang, and H. J. Sun, "Design of a w-band full-polarization monopulse cassegrain antenna," *IEEE Antennas Wireless Propag. Lett.*, vol. 16, pp. 99–103, 2017.

[45] G.-L. Huang, S.-G. Zhou, and T.-H. Chio, "Highly-efficient self-compact monopulse antenna system with integrated comparator network for rf industrial applications," *IEEE Trans. Ind. Electron.*, vol. 64, no. 1, pp. 674–681, 2017.

[46] P. Zheng, B. Hu, S. Xu, and H. Sun, "A w-band high-aperture-efficiency multipolarized monopulse cassegrain antenna fed by phased microstrip patch quad," *IEEE Antennas Wireless Propag. Lett.*, vol. 16, pp. 1609–1613, 2017.

[47] Y. J. Cheng, W. Hong, and K. Wu, "Broadband self-compensating phase shifter combining delay line and equal-length unequal-width phaser," *IEEE Trans. Microw. Theory Techn.*, vol. 58, no. 1, pp. 203–210, 2010.

[48] F. Fan, J. Yang, V. Vassilev, and A. U. Zaman, "Bandwidth investigation on half-height pin in ridge gap waveguide," *IEEE Trans. Microw. Theory Techn.*, vol. 66, no. 1, pp. 100–108, 2018.

[49] D. Sun, X. Chen, L.-X. Guo, W. Cui, and J.-Y. Deng, "Hard–soft groove gap waveguide based on perpendicularly stacked corrugated metal plates," *IEEE Trans. Microw. Theory Techn.*, vol. 69, no. 8, pp. 3684–3692, 2021.

[50] M. Ferrando-Rocher, J. I. Herranz-Herruzo, A. Valero-Nogueira, and M. Baquero-Escudero, "Half-mode waveguide based on gap waveguide technology for rapid prototyping," *IEEE Microw. Wireless Compon. Lett.*, vol. 32, no. 2, pp. 117–120, 2022.

[51] M. Ferrando-Rocher, J. I. Herranz-Herruzo, A. Valero-Nogueira, and M. Baquero-Escudero, "A half-mode groove gap waveguide for single-layer antennas in the millimeter-wave band," *IEEE Antennas Wireless Propag. Lett.*, vol. 21, no. 12, pp. 2402–2406, 2022.

[52] A. Colzani, M. Fumagalli, A. Fonte, A. Traversa, and E. Ture, "Long-reach e-band hpa for 5g radio link," in *2022 52nd EuMC*, 2022, pp. 760–763.